Accepted Manuscript

Title: The Farsund intrusion (SW Norway): A marker of Late-Sveconorwegian (Grenvillian) tectonism emplaced along a newly defined major shear zone

Authors: Olivier Bolle, Hervé Diot, Jean-Paul Liégeois, Jacqueline Vander Auwera

PII: S0191-8141(10)00050-7

DOI: 10.1016/j.jsg.2010.04.003

Reference: SG 2438

To appear in: *Journal of Structural Geology*

Received Date: 4 November 2009

Revised Date: 2 April 2010

Accepted Date: 11 April 2010

Please cite this article as: Bolle, O., Diot, H., Liégeois, J.-P., Auwera, J.V. The Farsund intrusion (SW Norway): A marker of Late-Sveconorwegian (Grenvillian) tectonism emplaced along a newly defined major shear zone, Journal of Structural Geology (2010), doi: 10.1016/j.jsg.2010.04.003

The Farsund intrusion (SW Norway): a marker of Late-Sveconorwegian (Grenvillian) tectonism emplaced along a newly defined major shear zone

Olivier Bolle [a, *, 1], Hervé Diot [b], Jean-Paul Liégeois [c] and Jacqueline Vander Auwera [a]

[a] *Dpt. de Géologie, Université de Liège, Bd. du Rectorat – Bât. B20, B-4000 Sart Tilman, Belgium*

[b] *Pôle Sciences et Technologie, Université de La Rochelle, Av. M. Crépeau, F-17042 La Rochelle Cedex 01, France*

[c] *Isotope Geology Division, Royal Museum for Central Africa, B-3080 Tervuren, Belgium. Jean-paul.liegeois@africamuseum.be*

Submitted to the Journal of Structural Geology

Abstract

The ca. 930 Ma Farsund intrusion (SW Norway) belongs to a series of 0.99-0.92 Ga post-collisional plutons from the Sveconorwegian (Grenvillian) orogen. It is made of two rock facies (charnockite and quartz mangerite, and subordinate quartz monzonite and quartz monzodiorite) that show mingling relationships. As shown elsewhere, these two facies belong, respectively, to the two suites of A-type affinity recognized in the Sveconorwegian post-collisional magmatism of Southern Norway, namely the AMC and HBG suites. A structural study of the Farsund intrusion, based on the anisotropy of magnetic susceptibility (AMS) technique, is presented here. The AMS is controlled by the shape-preferred orientation of low-Ti titanomagnetite grains and it can be used as a proxy for the global petrofabric. The AMS data, when combined with micro- to macrostructural observations, unfold the occurrence of a steeply-dipping shear zone, straddling the NE border of the pluton and characterized by a likely strike-slip component of shearing. This high-strain zone is roughly coincident with the boundary between the outcrop domains of the AMC and HBG suites, and was formed or, more probably, reactivated during the gravitational collapse of the Sveconorwegian orogen, in an extensional (possibly transtensional) tectonic regime. It would have controlled the ascent and emplacement of the Farsund intrusion, and materializes as well the structural weakness that would have channelled the magmas of the neighbouring and coeval Rogaland anorthosite province (RAP). It is also suggested that vertical, gravity-driven movements were recorded in the Farsund intrusion and its close surroundings. They would have been induced in a very hot environment, akin to that prevailing in the Precambrian ultra-hot orogens, but linked in the present case to the emplacement of anorthosites and penecontemporaneous igneous bodies, including the Farsund intrusion.

Keywords: Anisotropy of magnetic susceptibility; Charnockite; Granite emplacement; Transtension; Gravity tectonism; Sveconorwegian orogen

* Corresponding author. Tel: +32 4 3662260. Fax: +32 4 3662921. *E-mail address*: olivier.bolle@ulg.ac.be (O. Bolle).

[1] Research Associate from the F.N.R.S., Belgium.

1. Introduction

Granitoids occupy an important volume of the continental crust, especially in orogenic belts, and they represent key markers of the Earth's crust evolution. In particular, it is now well established that granitic plutons are syntectonic in many cases and, hence, that they may be used as markers of crustal deformation at the time of their emplacement, since they are capable of recording tectonic strain in the course of their crystallization, down to solid-state conditions (see the review in Bouchez, 2000). The use of the anisotropy of magnetic susceptibility (AMS) technique (e.g. Rochette *et al.*, 1992; Borradaile and Jackson, 2004) in the structural mapping of granitic plutons has greatly contributed to demonstrate the common syntectonic nature of granitoid emplacement (Bouchez *et al.*, 1990; Archanjo *et al.*, 1994; de Saint Blanquat and Tikoff, 1997; Ferré *et al.*, 1997; Gleizes *et al.*, 1997; Trindade *et al.*, 1999; Benn *et al.*, 2001; Bolle *et al.*, 2003b; Román-Berdiel *et al.*, 2004; Čečys and Benn, 2007; Joly *et al.*, 2007; Henry et *al.*, 2009; among others). In granitoids, the AMS, which is one of various types of magnetic fabrics, arises mostly from the crystallographic- and/or shape-preferred orientation of the magnetic rock-forming minerals; it is representative, in many cases, of the global, usually ill-defined petrofabric which, therefore, can be determined accurately through AMS measurements (Bouchez, 1997, 2000).

We have applied the AMS technique to the ca. 930 Ma Farsund intrusion (Falkum and Petersen, 1974; Falkum *et al.*, 1979; Dupont *et al.*, 2005), which belongs to a series of post-collisional plutons that intruded the Sveconorwegian orogen, a segment of the Grenvillian belt exposed in Southern Norway and SW Sweden, during the early Neoproterozoic (0.99-0.92

Ga). The Farsund intrusion, quite famous in igneous petrology since the term "farsundite" has been proposed as a synonym for hypersthene granite or charnockite (Streckeisen, 1974; but see Wilson, 1977), is supposed to have escaped regional folding (Falkum, 1985, 1998). It is a potentially important marker of the structural and petrological evolutions of the Sveconorwegian post-collisional magmatism, given its likely location near a major lithotectonic boundary (Duchesne *et al.*, 1999; Vander Auwera *et al.*, subm.).

2. Geological setting

2.1. The Sveconorwegian orogen

The Sveconorwegian orogen forms the southwestern, youngest portion of the Baltic Shield (the exposed part of Fennoscandia; Fig. 1a). This orogen is covered by Caledonian nappes to the west and is truncated by the Late Carboniferous–Permian Oslo graben in its central part. It is divided into several N-S to NW-SE–trending crustal segments (or terranes) made of Paleo- to Mesoproterozoic crust reworked during the 1.14-0.90 Ga Sveconorwegian orogeny (Bingen *et al.*, 2008b; Bogdanova *et al.*, 2008) and separated by major shear-zones. Models of terrane juxtaposition during the Sveconorwegian orogeny (see Bingen *et al.*, 2005, 2008b for recent contributions and references) evoke thrusting of allochton terranes on the easternmost, parautochtonous domain of the orogen and large, sinistral relative displacements between these terranes along the N-S–trending orogen-parallel shear zones, during collision between the SW margin of Fennoscandia and another major plate, possibly Amazonia. The strike-slip component of movement points to an oblique collision and indicates a transpressive tectonic regime at the orogen scale.

Numerous post-collisional plutons, dated at 0.99-0.92 Ga (compilation of U-Pb ages and new data in Bingen *et al.*, 2008b), occur in the Sveconorwegian orogen (Fig. 1a). They are dominated by biotite or hornblende + biotite (rarely biotite + muscovite), metaluminous to slightly peraluminous granitoids (Bogaerts *et al.*, 2003; Eliasson *et al.*, 2003; Vander Auwera *et al.*, 2003). These granitic plutons form two roughly N-S–trending belts across the orogen (Fig. 1a). The first belt (Andersen *et al.*, 2001; Eliasson *et al.*, 2003), to the east, encompasses three major plutons (the Flå, Iddefjord and Bohus granites) that are elongated parallel to the boundary of two terranes. The second belt (Andersen *et al.*, 2001; Vander Auwera *et al.*, 2003, 2008), to the west, is larger and occurs mostly to the west of the Mandal–Ustaoset Line, a lineament materialized by faults and shear zones that is generally regarded as a lithospheric-scale discontinuity (Sigmond, 1985; Bingen and van Breemen, 1998). Anorthosite to charnockite plutons occur to the SW of the western granitic belt (Duchesne *et al.*, 1985; Duchesne, 2001; see also next section).

The post-collisional plutons were mostly emplaced during the 0.97-0.90 Ga Dalane phase, as defined by Bingen *et al.* (2008b) in their four-phase model of the Sveconorwegian orogeny. The Dalane phase corresponds to a gravitational collapse of the orogen, characterized by core complex and gneiss dome formation (Bingen *et al.*, 2006), and ductile to brittle normal reactivation or overprinting of the major shear-zones (Andréasson and Rodhe, 1990; Starmer, 1993; Mulch *et al.*, 2005).

2.2. The Rogaland–Vest-Agder sector

The Farsund intrusion is exposed to the west of the Mandal–Ustaoset Line, in the Rogaland–Vest-Agder sector (Fig. 1a, b). This sector consists of a high-grade gneiss complex, intruded by several post-collisional plutons.

The high-grade gneiss complex is made of three lithological units (Fig. 1b; Falkum, 1985, 1998): banded, granitic and augen gneisses. The banded gneiss consists of alternating quartzofeldspathic and mafic (amphibolite or metanorite) layers, typically 1- to 50-cm-thick and is variably migmatitic. It contains small bodies of amphibolite and pyroxene-rich gneisses, as well as intercalations of metasediments (garnetiferous gneiss and schist, metaquartzite, calc-silicate rocks, marble). The granitic gneiss is a locally augen-bearing, faintly-foliated orthogneiss. Available U-Pb dates of banded and granitic gneisses indicate protolith formation between 1.55 and 1.03 Ga (summary in Bingen *et al.*, 2008b). Most augen gneiss bodies are metamorphosed megacrystic granodiorite plutons of the syn-collisional (1.05 Ga) high-K calc-alkaline Feda suite (Fig. 1a; Bingen and van Breemen, 1998). A few minor augen gneiss bodies belong to the pre-collisional (1.19-1.15 Ga) A-type Gjerstad suite that occurs all-over Southernmost Norway (Zhou *et al.*, 1995; Bingen and van Breemen, 1998).

The post-collisional plutonism in the Rogaland–Vest-Agder sector is represented by two petrographically, chemically and geographically distinct suites of A-type affinity (Fig. 1b; Vander Auwera *et al.*, 2003): a hornblende + biotite ferro-potassic granitoid (HBG) suite described all over Southern Norway and an orthopyroxene-bearing or anorthosite-mangerite-charnockite (AMC) suite restricted to the Rogaland–Vest-Agder sector. The plutons defining the HBG suite belongs to the western granitic belt of the Sveconorwegian orogen (Fig. 1a). U-Pb geochronology dates their emplacement at 0.96-0.95 Ga in the Rogaland–Vest-Agder sector (Vander Auwera *et al.*, subm.), as best defined by the 950 ± 5 Ma Lyngdal granodiorite (Bogaerts *et al.*, 2003, 2006) and the 957 ± 7 Ma Holum monzogranite (Bolle *et al.*, 2003b; Bingen *et al.*, 2006) (see Fig. 1b for location). The AMC suite is defined by the Rogaland anorthosite province (RAP; Fig. 1b; Duchesne *et al.*, 1985; Duchesne, 2001), a huge igneous complex that mainly consists of four coalescent large intrusions (the Egersund-Ogna, Åna-

Sira and Håland-Helleren anorthosites, and the Bjerkreim-Sokndal layered intrusion, BKSK) and two outliers (the Hidra and Garsaknatt leuconorites). The RAP was built in a short period of time, at 0.93-0.92 Ga (U-Pb ages; Pasteels *et al.*, 1979; Schärer *et al.*, 1996; Vander Auwera *et al.*, subm.). Some composite plutons containing hornblende + biotite and orthopyroxene granitoids are found in the vicinity of the RAP (Fig. 1b). The Farsund intrusion, which extends the RAP towards the SE, is the most voluminous of them.

The metamorphic grade in the Rogaland–Vest-Agder gneiss complex increases westwards, from upper amphibolite to granulite facies, as reflected by a sequence of four isograds (Fig. 1b; Tobi *et al.*, 1985; Bingen *et al.*, 1996): clinopyroxene-in, orthopyroxene-in, osumilite-in and (inverted) pigeonite-in isograd. This isograd pattern results from the superposition of three Sveconorwegian metamorphic events, dated by U-(Th)-Pb geochronology (Möller *et al.*, 2003; Tomkins *et al.*, 2005; Bingen *et al.*, 2008a): M1, a medium-P, regional metamorphic stage linked to crustal thickening (1.035-0.97 Ga); M2, a low-P – high- to ultra-high-T stage induced by the multi-emplacement of the RAP (0.93-0.92 Ga); M3, a low-P retrograde stage related to post-M2 cooling. U-(Th)-Pb data also demonstrates that the orthopyroxene isograd is a composite M1–M2 isograd, while the pigeonite, osumilite and clinopyroxene isograds relate to M2 (Möller *et al.*, 2003; Bingen *et al.*, 2008a). This latter phase represents a major thermal event, reflecting the superimposition of penecontemporaneous magmatic heat pulses, for which various geothermobarometres indicate peak temperatures of 800°C to > 1000°C close to the RAP and 700-750°C in the vicinity of the orthopyroxene isograd, at pressures of about 5 kbar (Wilmart and Duchesne, 1987; Holland *et al.*, 1996; Westphal *et al.*, 2003; and references therein).

The high-grade gneisses were affected by at least four to six phases of folding (Huijsmans *et al.*, 1981; Falkum, 1985, 1998; Starmer, 1993). The first, most probably pre-Sveconorwegian and composite phase produced mesoscopic to large-scale isoclinal folds with axial plane foliation, whereas the next phases gave rise to N-S–trending large-scale folds, with gradually greater interlimb angles (isoclinal to close folds), steeper axial planes (presumably recumbent to upright folds) and smaller amplitudes. These superimposed folds are coeval with high-grade metamorphism. The last phase of deformation is an exception, since it produced gentle to open large-scale folds, commonly along E-W axes and, apparently, without any related metamorphic recrystallization. Following Falkum (1998), most superimposed folds, with the notable exception of the latest ones, successively developed along the same N-S–trending axis, in response to syn-orogenic E-W horizontal shortening.

The emplacement of both the HBG and AMC suites in the Rogaland–Vest-Agder sector is coeval with regional-scale ductile deformation, responsible for some of the youngest folds observed in the high-grade gneiss complex (Falkum, 1998; Bolle *et al.*, 2003b; Bingen *et al.*, 2006). Ductile, gravity tectonism within the RAP, namely diapiric emplacement of the Egersund-Ogna, Åna-Sira and Håland-Helleren anorthosites (Duchesne *et al.*, 1985; Barnichon *et al.*, 1999) and gravity-driven subsidence of the BKSK (Paludan *et al.*, 1994; Bolle *et al.*, 2000, 2002), is also a well established feature. All these evidence for late-Sveconorwegian ductile deformation overlapping with post-collisional plutonism were taken by Bingen *et al.* (2006) as arguments, among other evidence, to interpret the Rogaland–Vest-Agder high-grade domain as a large-scale gneiss dome, progressively exhumed between 0.96 and 0.92 Ga, during, and possibly triggered by, the production of the HBG and AMC suites.

3. Petrology and field structural description of the Farsund intrusion and its country rocks

The Farsund intrusion is a NW-SE elongated pluton which crops out over an area of ca. 105 km^2, on peninsulas and islands that are separated from each other by fjords (Fig. 2). The country rocks to the north consist of alternating units of banded and granitic gneisses, with a major body of augen gneiss (the Feda gneiss) belonging to the 1.05 Ga Feda suite. To the south, the intrusion is flanked by banded gneisses. The gneisses are in amphibolite facies to the NE, and in granulite facies to the NW and to the south (Falkum *et al.*, 1979; Falkum, 1982, 1998). The southern banded gneisses are partly covered by Quaternary moraines and, opposing most geological maps (e.g. Middlemost, 1968; Falkum *et al.*, 1979), we propose that these deposits also hide a portion of the Farsund intrusion (Fig. 2; see argument below). The intrusion borders the Lyngdal granodiorite and the Hidra leuconorite, respectively to the SE and to the NW, and is locally separated from these two plutons by a thin septum of gneiss (Fig. 2; Falkum *et al.*, 1972, 1979; Marker *et al.*, 2003).

The Farsund intrusion is made of two intermingled facies, i.e. two facies showing mingling relationships, whose petrography and spatial distribution cannot be shown on Fig. 2 and will be detailed below: a dominant dark facies containing orthopyroxene (here referred to as Opx facies), and a subordinate light facies containing hornblende and biotite (here referred to as Hbl + Bt facies). Both facies display relatively coarse-grained varieties (charnockite and quartz mangerite vs. mostly quartz monzonite, with grain size ≤ ca. 1 cm), that are locally intermingled with several-dm- to some-km-sized finer-grained bodies (charnockite and quartz mangerite vs. mostly quartz monzodiorite, with grain size ≤ ca. 5 mm). The coarser-grained varieties also contain cm- to some-dm-large mafic microgranular enclaves. Zircon U-Pb geochronology gives similar ages for the two facies (931 ± 2 Ma for the Opx facies and 926 ± 4 Ma for the Hbl + Bt facies; Dupont *et al.*, 2005), confirming their coeval character. Whole-rock and mineral chemistry, and Sr and Nd isotope data further prove that the Opx and Hbl + Bt facies belong to the AMC and HBG suites, respectively (Dupont *et al.*, 2005). The AMC and HBG sources were thus both involved in the genesis of the Farsund magmas. The age of ca. 930 Ma also implies that the emplacement of the Farsund intrusion is contemporaneous with the multi-emplacement of the RAP and, thus, participated to the heat production responsible for the high- to ultra-high-T M2 metamorphic event.

The pluton contains numerous gneiss xenoliths of variable nature, that appear to come mainly from the banded gneisses. Most of these xenoliths are rather small (from a-few-cm- to 1-m-large). A huge gneiss body in the SE central part of the pluton (Fig. 2), dissected by the surrounding magmas, may represent a roof pendant or a remnant (pinnacle) of the underlying floor. Dykes of aplite and pegmatite are scarce, and always thin (cm- to dm-large).

A foliation and a mineral lineation, mainly defined by a shape-preferred orientation (SPO) of feldspars and mafic aggregates, are visible in the pluton. The mafic microgranular enclaves and the gneissic xenoliths are aligned with the foliation that is usually well-defined, contrary to the lineation which is only locally well-expressed (see below). The foliation dips are always steep and the strikes are dominantly NW-SE, except to the SW where they progressively rotate westwards from NW-SE, through E-W, to SW-NE, revealing folding of the southern part of the pluton (Fig. 2). Moreover, the SW-NE–striking foliations abut against the northern limit of the moraine cover, which may be taken as an argument for the occurrence of a pluton lobe under the Quaternary deposits, as we propose in Fig. 2. It is also worth noting that the exposed margins of the pluton seem to be generally steep, in agreement with the steeply-dipping foliations.

The SPO degree progressively increases to the NE, with mafic aggregates being more and more stretched and wrapped around feldspars, and it reaches a maximum in an up to 1.5-2-km-large zone along the contact with the high-grade gneisses. In this more deformed zone, strain localization (strong grain size reduction and very strong SPO, associated with L-fabrics or dm-scale close to isoclinal folds and ductile shear-zones) occurs at the margin and in narrow corridors. Well-defined lineations, as locally measured in the latter zones of strain localization, have plunges of ca. 30° towards the SE or SSE (Fig. 2). In the high-grade gneisses, gneissic foliations and mineral lineations concordant with the structures in the more deformed zone along the NE contact are found up to 1-2 km away from the margin (Fig. 2). Hence, our field structural observations unfold the occurrence of a few-km-large steeply-dipping and roughly linear belt, that straddles the NE border of the Farsund intrusion and which we interpret as a ductile shear zone (here referred to as *the Farsund shear zone*), given the obvious mylonitization of the pluton associated with it.

To the north of the pluton, outside the Farsund shear zone, the gneissic foliations and the most common types of lineations in the metamorphic envelope, namely mineral and crenulation lineations, exhibit a more complicated pattern, resulting from fold interference (Fig. 2; Falkum, 1998). To the south, the banded gneisses draw a large-scale antiform or dome, with associated mineral lineations that are gently to moderately plunging, predominantly to the NNE (Fig. 2). The foliation pattern in the south of the Farsund intrusion is concordant with this folded structure, at the map scale.

In summary, the Farsund intrusion is concordant with the regional structure observed in the gneisses near the margins: the pluton is elongated parallel to a steeply-dipping shear zone that straddles the NE margin (the Farsund shear zone) and it is concordant to a large-scale antiform or dome to the south. Let us note that the foliations in the Farsund intrusion are parallel to that measured in the huge gneiss body found in the SE central part of the pluton (Fig. 2).

The Lyngdal granodiorite, as the Farsund intrusion, exhibits a penetrative, usually steeply-dipping foliation. In the main E-W–trending body of the pluton (see location on Fig. 1b), the foliations are dominantly E-W–striking, whereas in the ca. N-S–striking limb extending to the north (Fig. 1b), they are NE-SW–striking in average (Fig. 2; Middlemost, 1968; Falkum *et al.*, 1979; Falkum, 1982). In the vicinity of the Farsund intrusion, the foliation strikes progressively evolve westwards from E-W to NNW-SSE or even N-S, and the foliation pattern is concordant with that of the Farsund intrusion and the banded gneisses to the SW (Fig. 2). However, around the city of Farsund, the foliations in the Farsund intrusion run parallel to the contact with the Lyngdal granodorite and are clearly oblique to the planar fabrics in the latter pluton (Fig. 2). In the same area, up to 1-m-large ductile shear zones, oblique to the earlier foliation, are locally observed in the Lyngdal granodiorite, up to 500-600 m away from the margin. These shear-zones are moderately- to steeply-dipping (ca. 50-80°) and are trending parallel to the contact with the Farsund intrusion. In agreement with Falkum *et al.* (1972, 1979), we conclude that the foliation deflection in the Farsund intrusion and the shearing in the Lyngdal granodiorite, as locally observed along the contact between the two plutons, were induced during emplacement of the ca. 930 Ma Farsund intrusion and its expansion at the expense of the already crystallized ca. 950 Ma Lyngdal granodiorite. Moreover, N- to ENE–plunging mineral lineations with moderate to steep plunges occur around the Farsund city, on each side of the contact between the Farsund intrusion and the Lyngdal granodiorite (Fig. 2; Falkum *et al*., 1979), pointing to a common strain history for the two plutons, at least locally.

A few field observations conducted in the Hidra leuconorite reveal the occurrence of a N-S–striking and steeply-dipping, rough penetrative foliation, mainly defined by a SPO of orthopyroxene grains. The steeply-dipping foliation pattern in the Farsund intrusion is roughly concordant with that evidenced in the Hidra leuconorite, but is slightly deflected towards parallelism with the margin when approaching the leuconorite body (Fig. 2). Such a foliation deflection is associated with the development of a mylonitic zone in the Farsund intrusion, extending all along the eastern margin of the Hidra leuconorite, up to a few hectometres away from the contact (Fig. 2). This high-strain zone (here referred to as *the Hidra mylonitic zone*) is characterized, at the outcrop scale, by a grain size reduction and by strongly stretched mafic aggregates wrapped around feldspar porphyroclasts; quartz and feldspar ribbons are also observed in narrow corridors of strain localization. In the northern, tongue-like end of the Farsund intrusion (see location on Fig. 2), the mylonitization is superimposed on strained rocks from the Farsund shear zone, giving rise to very well-developed quartz and feldspar ribbons, and an extremely strong SPO. Geochronologically, the Farsund intrusion and the Hidra leuconorite are penecontemporaneous, at ca. 930 Ma (Pasteels *et al.*, 1979; Dupont *et al.*, 2005) and, at this stage of the study, we ascribe formation of the Hidra mylonitic zone to the emplacement of the Hidra leuconorite shortly after crystallization of the Farsund intrusion.

4. Sampling and analytical procedures

One hundred and twenty-five sites have been sampled for AMS measurements (Fig. 3; Table 1). Most of them (114) are located in the Farsund intrusion. Eleven localities were also sampled in the Lyngdal granodiorite, in the junction area between the main body and the northern limb of the pluton. The samples consist of oriented cylinders (25 mm in diameter), cored with a portable drill. A total of 261 cores was collected (usually two cores per site).

The upper part of each core has been cut, in the laboratory, into two, rarely one, 22-mm-high cylinder(s), providing 520 specimens (usually four per site). The AMS of each specimen was measured, in a low magnetic field, using the Kappabridge KLY–3S susceptometer of AGICO Ltd. Measurements provided the magnitude and orientation of the three principal axes of the ellipsoid describing AMS in a low magnetic field ($K_1 \geq K_2 \geq K_3$). An average ellipsoid was calculated from the AMS measurements, for each sampling site, following the tensor averaging method of Hext (1963).

The lower part of the cores were used to make (sometimes polished) thin sections, in order to characterize the petrography of each sampling site. Thin sections from forty-three hand-size samples from the Farsund intrusion (most of them analyzed for geochemical purpose by Dupont, 2004) were also integrated in the present study.

5. Petrography and microstructural description of the sampled area

5.1. Petrography and mineral chemistry

Our microscope examination of the AMS samples confirms and completes previous petrographical descriptions of the Farsund intrusion and the Lyngdal granodiorite (Middlemost, 1968; Falkum *et al.*, 1979; Bogaerts *et al.*, 2003, 2006; Dupont, 2004).

Alkali feldspar, plagioclase and quartz, as main rock-forming minerals, zircon, apatite, and sporadic allanite and sulfides (pyrite, pyrrhotite, chalcopyrite), as accessory minerals, are shared by all facies. Orthopyroxene, clinopyroxene, hornblende, biotite, titanite, ilmenite and magnetite are also present, as main or accessory minerals, but their occurrence and proportions vary according to the lithology (Table 1): (1) in the Opx facies, the Fe-Mg silicates are orthopyroxene, hornblende, and subordinate clinopyroxene and biotite, titanite is markedly absent, and ilmenite is usually dominating over magnetite; (2) in the Hbl + Bt facies, as well as in the Lyngdal granodiorite, the Fe-Mg silicates are hornblende, biotite (absent in some samples) and sporadic clinopyroxene, titanite is a notably abundant accessory in many samples, and magnetite is more abundant than in the Opx facies and it is dominating over ilmenite. The high magnetite vs. ilmenite ratio and the occurrence of titanite in the Hbl + Bt facies and the Lyngdal granodiorite reflect the oxidizing character of the HBG magmas (Vander Auwera *et al.*, 2003) from which they crystallized. Moreover, hornblende may be more or less abundant than orthopyroxene in the Opx facies, which allows to distinguish between an Opx + Hbl sub-facies (orthopyroxene content ≥ hornblende content) and a Hbl +

Opx sub-facies (hornblende > orthopyroxene, with biotite being locally a relatively abundant accessory; Table 1). Hornblende is usually dominating over biotite in the Hbl + Bt facies, as well as in the Lyngdal granodiorite (Table 1).

Quartz typically forms anhedral, usually irregular grains. Plagioclase is an oligoclase to basic andesine (An_{22-35}; Wilson, 1977; Falkum *et al.*, 1979; Bogaerts *et al.*, 2003, 2006; Dupont, 2004), that may be antiperthic in the Farsund intrusion. It is subhedral and locally weakly zoned. Alkali feldspar varies from microperthitic orthoclase to microperthitic microcline, the latter being extensively developed in the Lyngdal granodiorite only. Mesoperthite is also common in the Opx facies. Myrmekite intergrowths at feldspar grain boundaries are very abundant. Orthopyroxene is mostly ferrosilitic (Dupont, 2004), and occurs both as oikocrysts of inverted pigeonite and subhedral (locally prismatic) primary grains. Clinopyroxene in the Opx facies is augitic (Dupont, 2004) and forms exsolution lamellae in orthopyroxene, as well as small grains or granules. It is diopsidic in the Lyngdal granodiorite (Bogaerts *et al.*, 2003, 2006) and in the Hbl + Bt facies, where it is found only as small relic inclusions in hornblende. Hornblende belongs to the hastingsite-edenite group (Bogaerts *et al.*, 2003, 2006; Dupont, 2004). It makes up grains of variable size and shape (including oikocrysts), as well as, in the Opx facies, rims around the Fe-Ti oxides. Biotite is subhedral to euhedral. Titanite rims the oxides or is found as small, usually anhedral grains. Ilmenite is optically homogeneous, except in some samples from the Lyngdal granodiorite, where it shows tiny hematite exsolutions. Magnetite is a Ti-poor titanomagnetite (Dupont, 2004) and exhibits evidence of subsolidus reactions (mostly trellis and sandwich microstructures formed by ilmenite lamellae; Duchesne, 1972) that are common in the Farsund intrusion only. Apatite, locally zoned zircon and sporadic allanite make up small, usually euhedral grains.

The rock texture is subhedral in the Farsund intrusion, where it evolves from inequigranular to equigranular from the coarse-grained facies (average grain size of 2-4 mm), through the fine-grained-facies (ca. 1-2 mm), to the microgranular enclaves (ca. 500 µm). Chilled facies is common in the latter, with apatite needles and Fe-Ti oxide grains dispersed in the other minerals. Samples from the Lyngdal granodiorite are coarse-grained (average grain size of 2-5 mm) and display a subhedral inequigranular texture, with frequent phenocrysts of plagioclase and/or alkali feldpsar, up to ca. 1-cm-long. In the coarse-grained rocks, aggregation of the Fe-Mg silicates and other accessory minerals, into more or less elongated clusters, is usually a rule.

Alteration is weakely developed, except in a few samples. It is expressed by damouritisation of feldspars, transformation of orthopyroxene into an orange-brown to rusty mineral (possibly iddingsite; Falkum *et al.*, 1979) plus pyrite or magnetite, chloritization of biotite (chlorite being accompanied by sericite, pistachitic epidote, calcite and/or pyrite in the Hbl + Bt facies and in the Lyngdal granodiorite) and corrosion of pyrite by a rusty rim (possibly Fe-hydroxide). Microfractures filled with chlorite, calcite, magnetite or pyrite locally cut across the mineral assemblage.

5.2. Distribution of the petrographic facies in the Farsund intrusion

A large zone of Hbl + Bt facies occurs in the west of the pluton and seems to be distributed along the trend of the folded pattern drawn by the foliations in the area. This facies is also observed along the western boundary of the huge gneiss body in the SE central part of the pluton and, more locally, close to the NE margin in the Farsund shear zone (Fig. 3). The Hbl + Opx sub-facies tends to concentrate in the core of the pluton, while the Opx + Hbl sub-facies tends to occur mostly close to the margins, and to the north and south of the main zone of Hbl + Bt facies (Fig. 3). Hence, the Farsund intrusion displays a roughly defined zonation.

Most samples of the Hbl + Opx sub-facies that are spatially associated with the Hbl + Bt facies actually belong to the HBG suite (Fig. 3), despite they contain orthopyroxene, as demonstrated by chemical (whole-rock and mineral) and isotopic (Sr and Nd) data obtained at the AMS sites, either on hand-size samples or on the AMS samples themselves (Dupont, 2004; Vander Auwera and Bolle, work in progress). For example, the hornblende Fe# [Fe/(Fe+Mg) cationic ratio] in the Hbl + Bt facies and in the associated Hbl + Opx sub-facies are similar (0.59-0.65, down to 0.45 in titanite-bearing rocks), but lower to that of the Opx + Hbl and Hbl + Opx sub-facies, as found elsewhere in the pluton (0.73-0.81). A complete geochemical investigation of the Farsund intrusion is outside the scope of the present study and will be conducted in a separated paper (Vander Auwera and Bolle, work in progress). Finally, fine-grained lithologies make an important part of the HBG zones, while fine-grained AMC rocks are anecdotal (Fig. 3; Table 1).

5.3. Microstructures

Minerals from the two sampled plutons display various *microscope-scale evidence of ductile deformation*. The quartz microstructure ranges from a slight undulose extinction to a well-defined pattern of subgrains (Fig. 4a, b). The largest grains of alkali feldspar and plagioclase are also frequently undulatory. Curvature of polysynthetic twins in the plagioclase is quite common, but usually weak (Fig. 4c), and very rare mechanical twins are also observed in this mineral. Slight curvature or kinking may affect some primary grains of orthopyroxene (Fig. 4d). In addition, the quartz-quartz and feldspar-feldspar grain boundaries are commonly serrated, suggesting dynamic recrystallization through high-T grain boundary migration (Hirth and Tullis, 1992; Passchier and Trouw, 2005). The high-T conditions of the deformation (>500-600°C) is also attested by frequent irregular quartz-feldspar grain boundaries (Fig. 4e), the dominantly square shape of quartz subgrains (Fig. 4a) and the abundance of myrmekites (Passchier and Trouw, 2005; and references therein). Such high temperatures are coherent with a ductile strain acquired at the end of or shortly after magma crystallization and also comply, at least for the Farsund intrusion, with the thermal conditions of the high- to ultra-high-T M2 metamorphic event. Quartz grains with elongated subgrains, usually occurring together with grains that display square-shaped subgrains, are also locally observed, essentially in the Lyngdal granodiorite (Fig. 4b), pointing to deformation at slightly lower temperatures (Passchier and Trouw, 2005).

In the Farsund shear zone, microstructural peculiarities, compared to less-deformed areas, are mostly observed in the zones of strain localization (narrow corridors and along the margin) and consist of a higher rate of intracrystalline deformation in quartz and feldspars, and an increase of the number of quartz grains with elongated subgrains. In the portion of the Lyngdal granodiorite affected by the emplacement of the Farsund intrusion, microstructural peculiarities consist of locally well-developed elongated subgrains in large grains of quartz associated with abundant aggregates of small quartz grains (probably new grains developed by dynamic recrystallization made predominantly through subgrain rotation; Hirth and Tullis, 1992; Fig. 4b). Rocks from the Hidra mylonitic zone exhibit very peculiar microstructural features, namely a fine-grained matrix (average grain size of 0.5-1 mm) containing large grains of quartz and alkali feldspar (<1 cm) that range from more or less elongated porphyroclasts to ribbons with shape ratios of 1/3 up to 1/7 and which usually show few evidence of intracrystalline deformation (Fig. 4f); strongly ductily deformed porphyroclasts of plagioclase (1.5-3.5 mm) also occur sporadically. The occurrence of quartz and feldspar ribbons still indicates straining at high temperatures, but points to a stronger deformation followed by important static recrystallization (Passchier and Trouw, 2005).

No reliable kinematic indicators were observed in thin section, as well as in the field, neither in the Farsund shear zone, nor in the Hidra mylonitic zone. The scarcity of assymetrical markers and incompletely transposed elements is especially worth noting. Such a feature is typical of shear zones developed under high-grade conditions and can be largely attributed to a high recrystallization degree (Passchier *et al.*, 1990; Passchier and Trouw, 2005).

6. AMS study

6.1. AMS scalar parameters

The *bulk magnetic susceptibility*, $K_m = (K_1 + K_2 + K_3)/3$, ranges in the whole data set from 9.3 to 172.9 x 10^{-3} SI (Table 1), with an average of 32.8 ± 21.9 x 10^{-3} SI. Such high values (>>10^{-3} SI) indicate that the magnetic mineralogy is dominated by ferromagnetic minerals (Rochette *et al.*, 1992; Bouchez, 2000), namely titanomagnetite which is ubiquitous in the studied samples and has a ferrimagnetic behaviour given its low Ti content (e.g. Clark, 1997). The dominant contribution of low-Ti titanomagnetite to the bulk magnetic susceptibility has been established, through various techniques, in other AMC and HBG magnetite-bearing rocks from the area (Bolle *et al.*, 2000; Bolle *et al.*, 2003b).

Histograms of K_m show two distinct, only slightly overlapping populations in the Farsund intrusion (Fig. 5a): (1) the Opx facies, with similar average K_m values for the Opx + Hbl sub-facies (24.2 ± 3.9 x 10^{-3} SI) and the Hbl + Opx sub-facies (26.4 ± 10.5 x 10^{-3} SI), and (2) the Hbl + Bt facies, with a much higher average K_m value of 75.0 ± 42.3 x 10^{-3} SI. The overlapping of K_m values is defined mostly by some samples of the Hbl + Opx sub-facies belonging to the HBG suite, that have a higher magnetite content than their AMC counterparts (sites 40, 62, 65; Table 1). It is also worth noting that the highest K_m values (>100 x 10^{-3} SI) are found in titanite-bearing, fine-grained rocks, that have very high magnetite contents (sites 66b, 81, 87; Table 1). The K_m values for the Lyngdal granodiorite are similar to those of the coarse-grained representatives of the Hbl + Bt facies (Fig. 5a; Table 1), with an average of 62.3 ± 11.3 x 10^{-3} SI. It can be concluded here that there is a good correlation between K_m and the petrographic type (magnetite content), and, also, that K_m is a useful discriminant between the low-fO_2 AMC and high-fO_2 HBG suites, at least at the pluton scale. Accordingly, contouring of K_m in the sampled area (Fig. 5b) reveals areas of maximum values (>40 x 10^{-3} SI) corresponding to the HBG zones of the Farsund intrusion and to the Lyngdal granodiorite.

Interestingly, the contoured map of K_m fits the aeromagnetic anomaly map of the area (references in Olesen *et al.*, 2004), where the Lyngdal granodiorite and the western (main) HBG zone of the Farsund intrusion are outlined by strong positive anomalies, whereas the rest of the Farsund intrusion (mostly AMC rocks) is occupied by lower positive anomalies. The positive aeromagnetic anomalies over the Farsund intrusion and the Lyngdal granodiorite are thus induced anomalies, whose intensity varies according to the magnetite content of the rocks. Such a conclusion complies with the results of McEnroe *et al.* (2001) which have shown that, in the RAP, rocks rich in multi-domain magnetite are related to positive magnetic anomalies induced by the present Earth's field, whereas rocks rich in hemo-ilmenite cause negative anomalies related to magnetic remanence acquired during a time of reversed magnetic polarity.

The *anisotropy degree* and *shape* of the magnetic fabric are expressed here using the P_j and T_j parameters of Jelinek (1981), respectively:

$$P_j = \exp\sqrt{2\sum_i (\ln K_i / K_m)^2} \text{ (i = 1 to 3) and } T_j = (2\ln K_2 - \ln K_1 - \ln K_3)/(\ln K_1 - \ln K_3),$$

where P_j expresses the departure from an undeformed, spherical AMS ellipsoid (P_j = 1), and T_j indicates a prolate (neutral, oblate) ellipsoid for $-1 \leq T_j < 0$ ($T_j = 0$, $0 < T_j \leq 1$).

The P_j values are in the interval 1.10–2.08 (Table 1), with an average of 1.33 ± 0.15, which means that moderately anisotropic magnetic fabrics dominate the data set. In a P_j vs. K_m diagram, the Lyngdal granodiorite defines a trend characterized by an increase of P_j with increasing K_m (Fig. 6a), a relationship that is common in magnetite-bearing granitoids and can be attributed, at least partly, to interactions between ferromagnetic grains (Bouchez, 2000). Such a positive correlation between P_j and K_m is a bit more roughly defined for the Hbl + Bt facies and is not obviously displayed for the Opx facies (Fig. 6a). For the latter facies, samples coming from the Hidra mylonitic zone and from areas of strain localization in the Farsund shear zone are shifted towards high P_j values in the P_j vs. K_m diagram (Fig. 6a). The P_j parameter is thus also related, at least locally, to the amount of strain undergone by the rocks. The competiting effects of the magnetic susceptibility (magnetite content) and deformation rate on the anisotropy degree is well illustrated on a contoured map of P_j (Fig. 6c): areas of maximum values (>1.4) are observed in the Lyngdal granodiorite and in the western (main) HBG zone of the Farsund intrusion, and also in the Farsund shear zone and in the Hidra mylonitic zone, with peak values (>1.8) in the strongly-strained, northern tongue-like end of the pluton.

The T_j parameter varies from -0.94 to 0.68 (Table 1), with an average of -0.39 ± 0.37, indicating that the magnetic fabric is dominantly prolate. A T_j vs. P_j diagram (Fig. 6b) and comparison of a contoured map of T_j (Fig. 6d) with Fig. 5b indicate that the shape of the magnetic fabric is not related to its anisotropy degree, nor to the bulk magnetic susceptibility (magnetic content). Actually, this parameter simply relates essentially to the shape of the magnetite grains. Indeed, since magnetite dominates the magnetic susceptibility, the magnetic fabric is mainly related to the subfabric of this oxide, which means that the AMS primarily results from the SPO of the ferrimagnetic grains (Archanjo *et al.*, 1995; Grégoire *et al.*, 1998; Launeau and Cruden, 1998). The contouring of T_j (Fig. 6d) further shows that strongly prolate magnetic fabrics (T_j > 0.5; strongly elongated magnetite grains) are mainly concentrated in the core of the Farsund intrusion and that oblate magnetic fabrics (T_j > 0; flattened magnetite grains) are mostly found in the vicinity of the Hidra leuconorite and in the Lyngdal granodiorite, at some distance of the Farsund intrusion.

6.2. AMS directional data

The pattern of the magnetic foliations (planes perpendicular to the K_3 axes) in the Farsund intrusion (Fig. 7) mimics that of the field foliations (Fig. 2) and, consequently, the average orientations of the magnetic and field foliations are very similar (N138E/87SW for the former and N146E/89NE for the latter; equal-area projections in Figs. 2, 7a). Slight to moderate obliquenesses are, however, locally observed in the central part of the pluton (Figs. 2, 7), but are probably not significant since the magnetic fabrics in the area are strongly prolate (foliations less defined than the lineations and, hence, more difficult to measure accurately; Fig. 6d). The AMS data further reveals that the foliations wrap around the huge gneiss body in the SE central part of the pluton. Such a deflection of the foliations is indicative of a more rigid behaviour of the gneiss body during deformation of the surrounding rocks. In the Lyngdal granodiorite, the orientations of the magnetic and field foliations are also similar (Figs. 2, 7). In particular, the AMS data confirm the dominantly NW-SE strikes of the foliations near the contact with the Farsund intrusion (concordance with the foliation pattern in the latter pluton, on the regional scale) and the E-W trend of the foliation pattern further east (Fig. 7).

The magnetic lineations (K_1 axes) in the Farsund intrusion are mostly moderately to steeply plunging towards the SE (Fig. 8) and their average orientation (N143E/67SE) is similar to that of the best-fit π-axis (N151E/75SSE) determined for the partial girdle defined by the magnetic foliation poles (equal-area projections in Figs. 7a, 8a), which confirms (cylindrical) folding of the pluton. Detailed inspection of Fig. 8 shows that the orientation of the magnetic lineations in the Farsund shear zone complies with that of the field lineations (Fig. 2): magnetic lineations are dominantly trending parallel to the NE margin, with gentle to moderate plunges (≤ ca. 50°) towards the SE or SSE. It also emerges from Fig. 8 that the magnetic lineations in the Farsund intrusion and the Lyngdal granodiorite, together with mineral lineations locally measured in both plutons and in the gneisses near the intrusive contacts define a single pattern characterized by: (1) a general steepening, from moderate (locally gentle) to steep (up to locally 85°) plunges, towards the southern border of the Farsund intrusion and (2) rotations, as seen in map view, in such a way that the lineation trajectories converge towards an area located at the SE end of the Farsund intrusion. The orientation of this pattern is modified in the Hidra mylonitic zone and close to it (Fig. 8). There, the lineations are dominantly steeply plunging towards W to NW or, in the northern tongue-like end of the Farsund intrusion and in the neighbouring high-grade gneisses, N to NE.

7. Magnetic fabric vs. petrofabric

The AMS scalar parameters provide some semi-quantitative informations on the studied rocks: K_m correlates with the magnetite content (AMC vs. HBG signature) and P_j is locally related to the strength of the petrofabric. The concordance of the magnetic foliations and lineations with the field foliations and lineations further indicates that the magnetic fabrics can be used as proxies for the petrofabrics and may help in revealing their significance. For instance, combination of the AMS directional data with the field and microscope structural observations show that the petrofabrics in the Farsund intrusion are no more purely magmatic: the widespread occurrence of microstructures attributed to mostly high-T, solid-state deformation, the continuity of the structures across the pluton and their concordance with those measured in the surrounding rocks (especially the continuity of the lineations across the pluton margins; Fig. 8b) demonstrate that a sub-solidus straining was superimposed onto the magmatic fabric, in continuity with the magmatic deformation. In the Farsund shear zone and in the Hidra mylonitic zone, sub-solidus straining and recrystallization are obviously extensive, whereas elsewhere in the pluton, the moderate imprint of the solid-state deformation, as revealed by the microstructural analysis, and the foliation deflection that is locally observed along the contact with the Lyngdal granodiorite (Figs. 2, 7) indicate that the rock texture is still partly inherited from the magmatic state.

Coaxiality between the magnetic fabrics, controlled by the SPO of minor magnetite grains and the rock shape fabrics, dominated by the SPO of silicates can now be justified, in the light of the magmatic- to solid-strain history established for the Farsund intrusion. The main reasons for such a correspondance are that: (1) magnetite, a liquidus mineral that started crystallizing early in the sequence of crystallization (Dupont, 2004), aligned preferentially parallel to the other crystals in the magma (as demonstrated through image analysis in other magnetite-bearing granitoids; Archanjo *et al.*, 1995; Launeau and Cruden, 1998) and (2) such a mimetic orientation has not been modified by sub-solidus straining and recrystallization, since both processes were operating in the continuity of the magmatic deformation. Coaxiality between magnetic fabrics and petrofabrics also requires magnetite grains being dominantly multi-domain (intrinsic maximum and minimum AMS axes parallel to the largest and shortest grain dimensions, respectively), which is the case here given magnetite grain size is usually

>20 μm (rough boundary between multi- and pseudo-single-domain magnetic behaviours in magnetite; Clark, 1997). Fine-grained secondary magnetite, as revealed by the petrographic analysis, is in trace amount and its influence on the magnetic fabrics is therefore negligible.

8. Structural control on the emplacement of the Farsund intrusion

The lineations in the steeply-dipping Farsund shear zone are predominantly gently to moderately-plunging (Figs. 2, 8), pointing to a strike-slip component of shearing. Indeed, one can safely consider that the magnetic and mineral lineations approximate the axis of maximum finite stretching, and it can also be assumed that they are relatively close to a solid-state flow (shear) direction, at least in the most strained rocks such as those of the Farsund shear zone. In absence of any reliable sense-of-shear marker, both the sense of strike-slip shearing (dextral or sinistral) and the dip-slip component of shearing (normal or inverse) cannot be determined. One can only assume a normal component, given the extensional tectonic regime that prevailed at the time of emplacement of the Farsund intrusion, i.e. during the Dalane phase of Bingen *et al.* (2008b) characterized regionally by the exhumation of the Rogaland–Vest-Agder sector as a large-scale gneiss dome (Bingen *et al.*, 2006). If this interpretation holds true, the Farsund shear zone would be a transtension structure.

In the northern tongue-like end of the Farsund intrusion and close to it, in the high-grade gneisses, the lineations are steeply-plunging (Figs. 2, 8), pointing to a different kinematics for the northern portion of the Farsund shear zone. As tackled above, rocks from the tongue-like end are extremely strained (very well-developed quartz and feldspar ribbons, extremely strong SPO and P_j values >1.8), as a consequence of the mylonitization along the eastern margin of the Hidra leuconorite, that was locally superimposed on strained rocks from the Farsund shear zone. The development of the Hidra mylonitic zone, that we ascribe to the emplacement of the Hidra leuconorite, is also responsible for the local steepening of the lineations and probably erased the likely strike-slip component recorded further south in the Farsund shear zone.

Actually, the structural pattern along the NE margin of the Farsund intrusion is quite similar to that observed at the eastern border of the RAP (Fig. 9a): (1) N-S– to NW-SE–striking, steeply-dipping foliations occur in a roughly linear, several-km-large zone that straddles the eastern margin of the RAP (Krause and Pedall, 1980; Falkum, 1982; Bolle *et al.*, 1997, 2000; Marker *et al.*, 2003) and (2) along that margin, a strong SPO with narrow corridors of strain localization is developed (Rietmeijer, 1979; Bolle *et al.*, 1997, 2000) in felsic rocks from the BKSK (quartz mangerites and charnockites forming the cap of the layered intrusion; Fig. 1b; Duchesne and Wilmart, 1997) and in the so-called Apophysis of the BKSK (a sheet-like igneous body, coeval with the BKSK felsic rocks, made of various intermingled felsic to jotunitic rocks and that is sandwiched between the Åna-Sira anorthosite and the high-grade gneisses; Fig. 1b; Bolle and Duchesne, 2007). Hence, there is a steeply-dipping shear zone that straddles the eastern border of the RAP, similar to the Farsund shear zone which runs along the NE margin of the Farsund intrusion. The Farsund shear zone can be viewed as a branch of this larger structure that will be here referred to as *the RAP shear zone* (Fig. 9a). Mineral and magnetic lineations in the RAP shear zone and close to it are dominantly steeply-plunging (Demaiffe, 1977; Bolle *et al.*, 1997, 2000; Vander Auwera *et al.*, 2006), as it is the case at the northern end of the Farsund shear zone. The usually steep nature of the lineations, as well as local variations in the orientation and thickness of the zone with steeply-dipping foliations in the gneisses (Fig. 9a), suggest that the emplacement of the RAP and the coeval to subsequent gravity tectonism (Duchesne *et al.*, 1985; Paludan *et al.*, 1994; Barnichon *et al.*, 1999; Bolle *et al.*, 2000, 2002) have restructured the RAP shear zone, erasing, in particular, any evidence of the likely strike-slip component that is recorded in the Farsund shear zone (this point will be discussed with more details in the next section).

The Farsund and RAP shear zones represent two branches of a major structure that had not been reported so far. However, the occurrence of a large-scale discontinuity to the east of the RAP has been envisaged by Duchesne *et al.* (1999) who stated that a lithospheric-scale weakness zone would be responsible for a large Moho offset identified to the south of the Farsund intrusion, on an offshore deep seismic profile (Andersson *et al.*, 1996). Duchesne *et al.* (1999) proposed that the N-S-elongated Feda gneiss (Fig. 9a) could materialize that weakness zone, in the same way as the Mandal gneiss, another N-S–striking representative of the Feda suite, seals the southward prolongation of the Mandal–Ustaoset Line (Fig. 1b). The linear aspect of the N-S–trending unit and the common occurrence of N-S–striking, gently-plunging lineations inside it (Falkum, 1998) agree with the idea of the Feda gneiss materializing a major (strike-slip) structure (Duchesne *et al.*, 1999). However, the gentle to moderate dips of the foliations and the folding of the southern tip of the gneiss body (Fig. 2) cannot be explained straightforward with this model. Hence, if the Feda gneiss is really elongated along a lithospheric-scale weakness zone, the latter was probably no longer active during the Dalane phase, contrary to the Farsund and RAP shear zones.

The close spatial association of the Farsund intrusion, as well as the RAP, with a major shear zone is certainly not accidental. Actually, the collocation of igneous bodies, especially granitic plutons, with large-scale shear zones and faults is common, and it is now widely admitted that these major structural weaknesses may control the upward transfer and emplacement of magmas in the crust (e.g. Hutton, 1988; D'Lemos *et al.*, 1992; Archanjo *et al.*, 1994; Ferré *et al.*, 1997; Brown and Solar, 1998; Liégeois *et al.*, 2003; Čečys and Benn, 2007; Joly *et al.*, 2007; Henry *et al.*, 2009). Such a model of tectonically-controlled magmatism applies to the Sveconorwegian post-collisional plutons: models of genesis, ascent and emplacement controlled by large-scale discontinuities were proposed for the Flå–Iddefjord–Bohus granitic belt (emplacement along the neighbouring terrane boundary; Fig. 1a; Andersson *et al.*, 1996; Eliasson *et al.*, 2003), for plutons of the western granitic belt (emplacement along the Mandal–Ustaoset Line; Fig. 1a; Vander Auwera *et al.*, 2003) and for the RAP (emplacement along the lithospheric-scale weakness zone detected through deep seismic data; see above; Duchesne *et al.*, 1999). We propose that the structural weakness materialized by the RAP and Farsund shear zones would have controlled not only the ascent and emplacement of the RAP magmas, but also that of the Farsund intrusion which extends the RAP towards the SE.

9. Evidence of gravity tectonism

The two events of gravity tectonism evidenced in the RAP, i.e. the diapiric emplacement of the Egersund-Ogna, Åna-Sira and Håland-Helleren anorthosites (Duchesne *et al*., 1985; Barnichon *et al*., 1999), and the gravity-driven subsidence of the BKSK (Paludan *et al.*, 1994; Bolle *et al.*, 2000, 2002) relay each other in time, although being partly coeval. Indeed, the BKSK was emplaced and crystallized on top of the anorthosites (Wilson *et al.*, 1996) and, following Bolle *et al.* (2002), its downward transfer was made through the sinking, into the surrounding low-density anorthosites and granulitic gneisses, of the high-density mafic floor of the layered intrusion (a cumulate series of noritic average composition, locally more than 7-km-thick, lying under the felsic rocks; Fig. 1b). Such a sinking was made possible through very high temperatures related to the multi-emplacement of the RAP and consequent crustal softening, and is indissociable from late upward transfer of the anorthosites.

We attribute the steepening of the lineations in the RAP shear zone to the latest gravity-induced vertical movements, i.e. the subsidence of the BKSK and the relative upward flow of the neighbouring anorthosites and granulitic gneisses. Hence, the RAP shear zone would have localized late, gravity-induced "readjustments" between bodies of contrasted densities (BKSK, anorthosites and granulitic gneisses). Intrusions such as the Hidra and Garsaknatt leuconorites, as well as the Apophysis (Fig. 9a) were emplaced late in the tectonomagmatic history of the RAP (Demaiffe, 1977; Bolle and Duchesne, 2007), probably concurrently with the late gravity-induced movements. Therefore, the roles played, in the genesis of the Hidra mylonitic zone and the associated steepening of the lineations, by the emplacement of the Hidra leuconorite and the late gravity-induced movements cannot be distinguished from each other.

The convergent aspect of the lineation trajectories towards an area where the lineations are very steeply-plunging, as observed in the SE part of the Farsund intrusion (Fig. 8b), is related to a syn- to post-emplacement vertical stretching which became localized at the triple junction between the Farsund intrusion, the Lyngdal granodiorite and the antiform or dome that affects the southern banded gneisses, and that we interpret as being also gravity-induced. This vertical stretching is associated with the folding of the Farsund intrusion along a steeply-plunging axis (sub-parallel to the average magnetic lineation; Figs. 7a and 8a), which in turn is probably coeval with the folding or doming of the southern banded gneisses. The fold geometry, especially the steeply-plunging axis, and the regional tectonic context prevailing at ca. 930 Ma (Bingen *et al.*, 2008b) preclude that the folding could result from syn-orogenic horizontal shortening, contrary to most folds evidenced in the high-grade gneiss complex (Falkum, 1998). Actually, the folding records the last generation of folds that affected the gneisses and whose representatives located close to the RAP are thought to be coeval with the multi-emplacement of the anorthosite province (Falkum, 1998). Based on the striking similarity between the observed lineation pattern and that typical of subsiding troughs, as the one evidenced in the BKSK (Fig. 9b), we propose that the folding of the Farsund intrusion and the associated vertical stretching reflect gravity-induced vertical movements that occurred in the hot environment developed near the RAP and its offshore extension (gravity and aeromagnetic anomalies indicate that the Sveconorwegian post-collisional plutons, including the RAP, extend offshore towards 80 km away from the coast; Fig. 1a; Andersson *et al.*, 1996; Olesen *et al.*, 2004). Interestingly, a 20-30-km-large offshore negative gravity anomaly, coupled to a negative magnetic anomaly, appears on geophysical maps immediately to the south of the Farsund intrusion (Olesen *et al.*, 2004) suggesting the occurrence in that area of a large offshore anorthosite body. It cannot be excluded that the stretching localized in the SE portion of the Farsund intrusion could correspond to a return (downward) flow (Barnichon *et al.*, 1999) developed during (late?) upward transfer of this anorthosite.

In summary, it is proposed that gravity-driven movements were localized along the eastern border of the RAP, as well as at the SE end of the Farsund intrusion. These vertical movements developed in a very hot environment linked to the multi-emplacement of the RAP and its offshore extension, which is also responsible for the M2 metamorphic event. The very high thermal conditions in and around the RAP, locally enhanced by the emplacement of the Farsund intrusion, and the related vertical movements might have lasted for a quite long period of time (several million years), as suggested by thermal modeling of the anorthosite emplacement (Westphal *et al.*, 2003). This probably explains why gravity tectonism would have erased, in the RAP shear zone, any evidence of the likely strike-slip (possibly transtensional) tectonism evidenced in the Farsund shear zone.

The gravity tectonism that was active at and after ca. 930 Ma in the RAP and, as suggested here, in its close surroundings is akin to that prevailing in the Archean orogenic crust and, more generally, in the Precambrian ultra-hot orogens (Chardon *et al.*, 2009). In the latter case, however, vertical movements were occurring at a much broader scale due to regional high heat flow and could have been triggered, at least in some cases, by horizontal shortening.

10. NW-SE– to E-W– versus N-S–trending structures

The structural database presented here needs to be improved by additional investigations, in particular to materialize the southern and northern extension of the Farsund and RAP shear zones, respectively. However, on the basis of the available structural data, some light can be shed on the geodynamical significance of the structural trend evidenced in the Farsund intrusion and its surroundings.

The Farsund and RAP shear zones represent a major discontinuity (the Farsund-RAP shear zone), belonging to the N-S to NW-SE–trending shear-zone network that cuts across the Sveconorwegian orogen (Fig. 1a) and which could represent a transpressional structure reactivated in the extensional (possibly transtensional as suggested here) tectonic regime that characterizes the Dalane phase of Bingen *et al.* (2008b). The Farsund-RAP shear zone could also materializes the limit of two distinct major lithotectonic units, as it is roughly coincident with the boundary between the outcrop areas of the AMC and HBG suites whose evolutions were controlled by two contrasted crustal contaminants (Bolle *et al.*, 2003a; Vander Auwera *et al.*, subm.). In turn, this suggests that the shear zone could be inherited from a pre-Sveconorwegian, Mesoproterozoic or Paleoproterozoic structure generated during the birth of the continental crust in the area (as old as 1.85 Ga, based on Nd model ages of high-grade gneisses; Menuge, 1988). The NW-SE strike of the structure, contrasting with the N-S trend of the Rogaland–Vest-Agder gneiss complex (Fig. 1b) and, at a larger scale, with that of the southern portions of Sveconorwegian shear-zones (Fig. 1a) points, moreover, to interference with the N-S–trending Sveconorwegian structures during reactivation. Alternatively, the NW-

SE strike might equally indicate that the Farsund-RAP shear zone would have formed during the Dalane phase and could be equivalent to a transfer or accomodation zone (also called "fault-domain boundary"; Schlische and Withjack, 2009), oblique to the main structural domains. This second hypothesis dismisses, however, a model considering the Farsund-RAP shear zone as a limit between two different pre-Sveconorwegian domains.

The E-W strike which characterizes the main body of the Lyngdal granodiorite (Fig. 1b) and most steeply-dipping foliations found inside it (Figs. 2, 7) represents an even greater anomaly in the predominantly N-S–trending structural pattern of the Rogaland–Vest-Agder sector. It is tempting to link this E-W trend to emplacement along a discontinuity that would be a satellite of the Sorgenfrei–Tornquist Zone, an E-W- to NW-SE–trending, large (20-45 km) and complex –mostly offshore– fracture zone cutting across the Precambrian basement and the Phanerozoic cover of the southwesternmost corner of Fennoscandia (Fig. 1a; Berthelsen, 1998; see also the review of Pharaoh, 1999). This intraplate major structure was mostly active during Late Palaeozoic and Mesozoic times, in the course of which successive tectonic phases gave rise to faults with normal and/or strike-slip component, and grabens (Pegrum, 1984; Liboriussen *et al.*, 1987; Mogensen, 1994). However, it has been argued that the Sorgenfrei–Tornquist Zone might have a much longer and more complex history, as it is often the case for lithospheric-scale structures, and already existed since Proterozoic time. Indeed, the Sorgenfrei–Tornquist Zone is believed to belong to a set of Precambrian lineaments cutting across the Fennoscandian basement (references in Pegrum, 1984). The elongation of offshore Sveconorwegian intrusive bodies along the Sorgenfrei–Tornquist Zone also implies that location of the fracture zone has been governed by structuring of the Proterozoic basement (Fig. 1a; Olesen *et al.*, 2004).

11. Conclusions

As shown elsewhere, the Farsund intrusion was constructed by coeval magmas belonging to the AMC and HBG suites, the two Sveconorwegian post-collisional magmatic suites of A-type affinity identified in Southern Norway. The bulk magnetic susceptibility, in the Farsund intrusion and the neighbouring Lyngdal granodiorite, correlates with the rock magnetite content and, hence, discriminates between the low-fO_2 (magnetite-poor) AMC and high-fO_2 (magnetite-rich) HBG rocks. Combination of the AMS data with the field and microscope structural observations further suggests that two structural events were active during and after emplacement of the Farsund intrusion.

First, the Farsund intrusion is elongated parallel to the here defined Farsund shear zone, a steeply-dipping structure that straddles the NE border of the pluton. This shear zone exhibits a likely strike-slip component of shearing and possibly corresponds to a transtension structure. It branches from the Rogaland anorthosite province (RAP) shear zone, a similarly steeply-dipping structure that straddles the eastern margin of the RAP. The Farsund-RAP shear zone represents a newly discovered large-scale zone of weakness, roughly coincident with the boundary between the outcrop domains of the AMC and HBG suites. It was active at the time of emplacement of the Farsund intrusion and the RAP, i.e. during the gravitational foundering of the Sveconorwegian orogen (the so-called Dalane phase). This major NW-SE–striking shear zone, oblique to the N-S–trending Sveconorwegian terrane boundaries, is either a new structure (oblique "fault-domain boundary"?) formed during the Dalane phase or, more probably, an inherited transpressional structure reactivated during this phase. In the latter case, it could be an interference between N-S–trending Sveconorwegian structures and discontinuities inherited from the crust generation in the area during the Mesoproterozoic or the Paleoproterozoic. In both cases, it is proposed that the Farsund-RAP shear zone would have controlled the ascent and emplacement of the Farsund intrusion and the RAP.

The RAP shear zone probably evolved as a zone of localization of gravity-induced deformation linked to vertical readjustements between bodies of contrasted densities (anorthosites, BKSK, granulitic gneisses). The Farsund intrusion has also recorded a syn- to post-emplacement vertical stretching that became localized to the SE of the pluton and which was possibly also gravity-induced. All these gravity-driven movements developed in a very hot environment, similar to that prevailing in the Precambrian ultra-hot orogens, but having here a local origin, the heat being supplied by the emplacement of anorthosites and coeval igneous bodies, including the Farsund intrusion.

Acknowledgements

Technical assistance was received from J.P. Cullus. Field work was partly funded by the F.N.R.S. (National Fund for Scientific Research, Belgium). Helpful suggestions by B. Bingen, and constructive comments by K. Benn and an anonymous reviewer were greatly appreciated.

References

Andersen, T., Andresen, A., Sylvester, A.G., 2001. Nature and distribution of deep crustal reservoirs in the southwestern part of the Baltic Shield: evidence from Nd, Sr and Pb isotope data on late Sveconorwegian granites. Journal of the Geological Society, London 158, 253-267.

Andersson, M., Lie, J.E., Husebye, E.S., 1996. Tectonic setting of post-orogenic granites within SW Fennoscandia based on deep seismic and gravity data. Terra Nova 8, 558-566.

Andréasson, P.G., Rodhe, A. 1990. Geology of the Protogine Zone south of Lake Vättern, southern Sweden: a reinterpretation. Geologiska Föreningens i Stockholm Förhandlingar 112, 107-125.

Archanjo, C.J., Bouchez, J.L., Corsini, M., Vauchez, A., 1994. The Pombal granite pluton: magnetic fabric, emplacement and relationships with the Brasiliano strike-slip setting of NE Brazil (Paraíba state). Journal of Structural Geology 16, 323-335.

Archanjo, C.J., Launeau, P., Bouchez, J.L., 1995. Magnetic fabric vs. magnetite and biotite shape fabrics of the magnetite-bearing granite pluton of Gameleiras (Northeast Brazil). Physics of the Earth and Planetary Interiors 89, 63-75.

Barnichon, J.D, Havenith, H., Hoffer, B., Charlier, R., Jongmans, D., Duchesne, J.C., 1999. The deformation of the Egersund-Ogna anorthosite massif, south Norway: finite-element modelling of diapirism. Tectonophysics 303, 109-130.

Benn, K., Paterson, S.R., Lund, S.P., Pignotta, G.S., Kruse, S., 2001. Magmatic fabrics in batholiths as markers of regional strains and plate kinematics: example of the Cretaceous Mt. Stuart Batholith. Physics and Chemistry of the Earth 26, 343-354

Berthelsen, A., 1998. The Tornquist Zone northwest of the Carpathians: an intraplate pseudosuture. Geologiska Föreningens i Stockholm Förhandlingar 120, 223-230.

Bingen, B., Davis, W.J., Hamilton, M.A., Engvik, A.K., Stein, H.J., Skår, Ø., Nordgulen, Ø., 2008a. Geochronology of high-grade metamorphism in the Sveconorwegian belt, S. Norway: U-Pb, Th-Pb and Re-Os data. Norwegian Journal of Geology 88, 13-42.

Bingen, B., Demaiffe, D., van Breemen, O., 1996. Rb-Sr isotopic signature of augen gneiss suites in the Sveconorwegian Province of SW Norway. In: Demaiffe, D. (Ed.), Petrology and Geochemistry of magmatic suites of rocks in the continental and oceanic crusts. U.L.B.-M.R.A.C., Bruxelles, pp. 161-174.

Bingen, B., Nordgulen, Ø., Viola, G., 2008b. A four-phase model for the Sveconorwegian orogeny, SW Scandinavia. Norwegian Journal of Geology 88, 43-72.

Bingen, B., Skår, Ø., Marker, M., Sigmond, E.M.O., Nordgulen, Ø., Ragnhildstveit, J., Mansfeld, J., Tucker, R.D., Liégeois, J.P., 2005. Timing of continental building in the Sveconorwegian orogen, SW Scandinavia. Norwegian Journal of Geology 85, 87-116.

Bingen, B., Stein, H.J., Bogaerts, M., Bolle, O., Mansfeld, J., 2006. Molybdenite Re-Os dating constrains gravitational collapse of the Sveconorwegian orogen, SW Scandinavia. Lithos 87, 328-346.

Bingen, B., van Breemen, O., 1998. Tectonic regimes and terrane boundaries in the high-grade Sveconorwegian belt of SW Norway, inferred from U-Pb zircon geochronology and geochemical signature of augen gneiss suites. Journal of the Geological Society, London 155, 143-154.

Bogaerts, M., Scaillet, B., Liégeois, J.P., Vander Auwera, J., 2003. Petrology and geochemistry of the Lyngdal granodiorite (Southern Norway) and the role of fractional crystallization in the genesis of Proterozoic ferro-potassic A-type granites. Precambrian Research 124, 149-184.

Bogaerts, M., Scaillet, B., Vander Auwera, J., 2006. Phase equilibria of the Lyngdal granodiorite (Norway): Implications for the origin of metaluminous ferroan granitoids. Journal of Petrology 47, 2405-2431.

Bogdanova, S.V., Bingen, B., Gorbatschev, R., Kheraskova, T.N., Kozlov, V.I., Puchkov, V.N., Volozh, Y.A., 2008. The East European Craton (Baltica) before and during the assembly of Rodinia. Precambrian Research 160, 23-45.

Bolle, O., Demaiffe, D., Duchesne, J.C., 2003a. Petrogenesis of jotunitic and acidic members of an AMC suite (Rogaland anorthosite province, SW Norway): a Sr and Nd isotopic assessment. Precambrian Research 124, 185-214.

Bolle, O., Diot, H., Duchesne, J.C., 1997. Anisotropie de la susceptibilité magnétique dans une intrusion composite de la suite charnockitique: l'apophyse du massif stratiforme de Bjerkreim-Sokndal (Rogaland, Norvège méridionale). Comptes Rendus de l'Académie des Sciences de Paris (Série IIa) 325, 799-805.

Bolle, O., Diot, H., Duchesne, J.C., 2000. Magnetic fabric and deformation in charnockitic igneous rocks of the Bjerkreim-Sokndal layered intrusion (Rogaland, Southwest Norway). Journal of Structural Geology 22, 647-667.

Bolle, O., Diot, H., Trindade, R.I.F., 2003b. Magnetic fabrics in the Holum granite (Vest-Agder, southernmost Norway): implications for the late evolution of the Sveconorwegian (Grenvillian) orogen of SW Scandinavia. Precambrian Research 121, 221-249.

Bolle, O., Duchesne, J.C., 2007. The Apophysis of the Bjerkreim-Sokndal layered intrusion (Rogaland anorthosite province, SW Norway): a composite pluton build up by tectonically-driven emplacement of magmas along the margin of an AMC igneous complex. Lithos 98, 292-312.

Bolle, O., Trindade, R.I.F., Bouchez, J.L., Duchesne, J.C., 2002. Imaging downward granitic magma transport in the Rogaland Igneous Complex, SW Norway. Terra Nova 14, 87-92.

Borradaile, G.J., Jackson, M., 2004. Anisotropy of magnetic susceptibility (AMS): magnetic petrofabrics of deformed rocks. In: Martín-Hernández, F., Lüneburg, C.M., Aubourg, C., Jackson, M. (Eds), Magnetic fabric: methods and applications. Journal of the Geological Society of London, Special Publications 238, pp. 299-360.

Bouchez, J.L., 1997. Granite is never isotropic: an introduction to AMS studies of granitic rocks. In: Bouchez, J.L., Hutton, D.H.W., Stephens, W.E. (Eds), Granite: from segregation of melts to emplacement fabrics. Kluwer, Dordrecht, pp. 95-112.

Bouchez, J.L., 2000. Anisotropie de susceptibilité magnétique et fabrique des granites. Comptes Rendus de l'Académie des Sciences de Paris, Sciences de la Terre et des Planètes 330, 1-14.

Bouchez, J.L., Gleizes, G., Djouadi, T., Rochette, P., 1990. Microstructures and magnetic susceptibility applied to emplacement kinematics of granites: the example of the Foix pluton (French Pyrenees). Tectonophysics 184, 157-171.

Brown, M., Solar, G.S., 1998. Granite ascent and emplacement during contractional deformation in convergent orogens. Journal of Stuctural Geology 20, 1365-1393.

Čečys, A., Benn, K., 2007. Emplacement and deformation of the ca. 1.45 Ga Karlshamn granitoid pluton, southeastern Sweden, during ENE-WSW Danopolonian shortening. International Journal of Earth Sciences 96, 397-414.

Chardon, D., Gapais, D., Cagnard, F., 2009. Flow of ultra-hot orogens: A view from the Precambrian, clues for the Phanerozoic. Tectonophysics, doi: 10.1016/j.tecto.2009.03.008.

Clark, D.A., 1997. Magnetic petrophysics and magnetic mineralogy: aids to geological interpretation of magnetic surveys. Journal of Australian Geology and Geophysics 17, 83-103.

Demaiffe, D., 1977. Les massifs satellites anorthosito-leuconoritiques d’Hidra et Garsaknatt : leur signification pétrogénétique. Annales de la Société Géologique de Belgique 100, 167-174.

de Saint Blanquat, M., Tikoff, B., 1997. Development of magmatic to solid-state fabrics during syntectonic emplacement of the Mono Creek Granite, Sierra Nevada batholith. In: Bouchez, J.L., Hutton, D.H.W., Stephens, W.E. (Eds), Granite: from segregation of melt to emplacement fabrics. Kluwer, Dordrecht, pp. 231-252.

D'Lemos, R.S., Brown, M., Strachan, R.A., 1992. Granite magma generation, ascent and emplacement within a transpressional orogen. Journal of the Geological Society, London 149, 487-490.

Duchesne, J.C., 1972. Iron-titanium oxide minerals in the Bjerkrem-Sogndal massif, South-western Norway. Journal of Petrology 13, 57-81.

Duchesne, J.C. (Ed.), 2001. The Rogaland intrusive massifs, an excursion guide. Norges geologiske undersøkelse Report 2001.29, Geological Survey of Norway, Trondheim.

Duchesne, J.C., Liégeois, J.P., Vander Auwera, J., Longhi, J., 1999. The crustal tongue melting model and the origin of massive anorthosite. Terra Nova 11, 100-105.

Duchesne, J.C., Maquil, R., Demaiffe, D., 1985. The Rogaland anorthosites: facts and speculations. In: Tobi, A. C., Touret, J.L.R. (Eds), The deep Proterozoic crust in the North Atlantic Provinces. Reidel, Dordrecht, pp. 449-476.

Duchesne, J.C., Wilmart, E., 1997. Igneous charnockites and related rocks from the Bjerkreim-Sokndal layered intrusion (Southwest Norway): a jotunite (hypersthene monzodiorite) - derived A-type granitoid suite. Journal of Petrology 38, 337-369.

Dupont, A., 2004. Pétrologie, géochimie et géochimie isotopique du massif de Farsund (Norvège) : implications pour le magmatisme AMCG. PhD Thesis. Department of Geology, Liège University, Belgium.

Dupont, A., Vander Auwera, J., Pin, C., Paquette, J.L., Bogaerts, M., 2005. Inefficiency of magma mixing and source heterogeneity in the genesis of granitoids: the example of the Farsund intrusion (southern Norway). Geophysical Research Abstracts 7, 04915.

Eliasson, T., Ahlin, S., Petersson, J., 2003. Emplacement mechanism and thermobarometry of the Sveconorwegian Bohus granite, SW Sweden. Geologiska Föreningens i Stockholm Förhandlingar 125, 113-130.

ACCEPTED MANUSCRIPT

Falkum, T., 1982. Geologisk kart over Norge, berggrunnskart Mandal – 1:250,000. Norges geologiske undersøkelse.

Falkum, T., 1985. Geotectonic evolution of southern Scandinavia in light of a late-Proterozoic plate-collision. In: Tobi, A. C., Touret, J.L.R. (Eds), The deep Proterozoic crust in the North Atlantic Provinces. Reidel, Dordrecht, pp. 309-322.

Falkum, T., 1998. The Sveconorwegian magmatic and tectonometamorphic evolution of the high-grade Proterozoic Flekkefjord complex, south Norway. Norges geologiske undersøkelse Bulletin 434, 5-33.

Falkum, T., Petersen, J.S., 1974. A three-fold division of the "Farsundite" plutonic complex at Farsund, southern Norway. Norsk Geologisk Tidsskrift 54, 361-366.

Falkum, T., Wilson, J.R., Annis, M.P., Fregerslev, S., Zimmermann, H.D., 1972. The intrusive granites of the Farsund area, South Norway. Norsk Geologisk Tidsskrift 52, 463-465.

Falkum, T., Wilson, J.R., Petersen, J.S., Zimmermann, H.D., 1979. The intrusive granites of the Farsund area, south Norway: Their interrelations and relations with the Precambrian metamorphic envelope. Norsk Geologisk Tidsskrift 59, 125-139.

Ferré, E., Gleizes, G., Djouadi, M.T., Bouchez, J.L., Ugodulunwa, F.X.O, 1997. Drainage and emplacement of magmas along an inclined transcurrent shear zone: petrophysical evidence from a granite-charnockite pluton (Rahama, Nigeria). In: Bouchez, J.L., Hutton, D.H.W., Stephens, W.E. (Eds), Granite: from segregation of melt to emplacement fabrics. Kluwer, Dordrecht, pp. 253-273.

Gleizes, G., Leblanc, D., Bouchez, J.L., 1997. Variscan granites of the Pyrenees revisited: their role as syntectonic markers of the orogen. Terra nova 9, 38-41.

Grégoire, V., Darrozes, J., Gaillot, P., Nédélec, A., Launeau, P., 1998. Magnetite grain shape fabric and distribution anisotropy vs rock magnetic fabric: a three-dimensional case study. Journal of Structural Geology 20, 937-944.

Henry, B., Liégeois J.P., Nouar, O., Derder, M.E.M., Bayou, B., Bruguier, O., Ouabadi, A., Belhai, D., Amenna, M., Hemmi, A., Ayache, M., 2009. Repeated granitoid intrusions during the Neoproterozoic along the western boundary of the Saharan metacraton, Eastern Hoggar, Tuareg shield, Algeria: An AMS and U–Pb zircon age study. Tectonophysics 474, 417-434.

Hext, G.R., 1963. The estimation of second-order tensors, with related tests and design. Biometrika 50, 353-373.

Hirth, G., Tullis, J., 1992. Dislocation creep regimes in quartz aggregates. Journal of Structural Geology 14, 145–159.

Holland, T.J.B., Babu, E.V.S.S.K., Waters, D.J., 1996. Phase relations of osumilite and dehydration melting in pelitic rocks: a simple thermodynamic model for the KFMASH system. Contributions to Mineralogy and Petrology 124, 383-394.

Huijsmans, J.P.P., Kabel, A.B.E.T., Steenstra, S.E., 1981. On the structure of a high-grade metamorphic Precambrian terrain in Rogaland, south Norway. Norsk Geologisk Tidsskrift 61, 183-192.

Hutton, D.H.W., 1988. Granite emplacement mechanisms and tectonic controls: inferences from deformation studies. Transactions of the Royal Society of Edinburgh, Earth Sciences 79, 245-255.

Jelinek, V., 1981. Characterization of the magnetic fabrics of rocks. Tectonophysics 79, T63-T67.

Joly, A., Chen, Y., Faure, M., Martelet, G., 2007. A multidisciplinary study of a syntectonic pluton close to a major lithospheric-scale fault – Relationships between the Montmarault granitic massif and the Sillon Houiller Fault in the Variscan French Massif Central: 1. Geochronology, mineral fabrics, and tectonic implications. Journal of Geophysical Research 112, B10104.

Jorde, K., Sigmond, E.M.O., Thorsnes, T., 1995. Geologisk kart over Norge, berggrunnskart Stavanger – 1:250,000. Norges geologiske undersøkelse.

Krause, H., Pedall, K.G., 1980. Fe-Ti mineralizations in the Åna-Sira anorthosite, Southern Norway. In: Siivola, J. (Ed.), Metallogeny of the Baltic shield. Finland Geological Survey Bulletin 307, pp. 56-83.

Launeau, P., Cruden, A.R., 1998. Magmatic fabric acquisition mechanisms in a syenite: results of a combined anisotropy of magnetic susceptibility and image analysis study. Journal of Geophysical Research 103, 5067-5089.

Liboriussen, J., Ashton, P., Tygesen, T., 1987. The tectonic evolution of the Fennoscandian Border Zone in Denmark. Tectonophysics 137, 21-29.

Liégeois, J.P., Latouche, L., Boughrara, M., Navez, J., Guiraud, M., 2003. The LATEA metacraton (Central Hoggar, Tuareg Shield, Algeria): behaviour of an old passive margin during the Pan-African orogeny. Journal of African Earth Sciences 37, 161-190.

Marker, M., Schiellerup, H., Meyer, G.B., Robins, B., Bolle, O., 2003. Geological map of the Rogaland anorthosite province – Scale 1:75000. In: Duchesne, J.C., Korneliussen, A. (Eds.), Ilmenite deposits and their geological environment. With special reference to the Rogaland Anorthosite Province. Norges geologiske undersøkelse, Special Publication 9, Plate 1.

McEnroe, S.A., Robinson, P., Panish, P.T., 2001. Aeromagnetic anomalies, magnetic petrology, and rock magnetism of hemo-ilmenite- and magnetite-rich cumulate rocks from the Sokndal Region, South Rogaland, Norway. American Mineralogist 86, 1447-1468.

Menuge, J.F., 1988. The petrogenesis of massif anorthosites: a Nd and Sr isotopic investigation of the Proterozoic of Rogaland/Vest-Agder, SW Norway. Contributions to Mineralogy and Petrology 98, 363-373.

Middlemost, E., 1968. The granitic rocks of Farsund, South Norway. Norsk Geologisk Tidsskrift 48, 81-99.

Mogensen, T.E., 1994. Palaeozoic structural development along the Tornquist Zone, Kattegat area, Denmark. Tectonophysics 240, 191-214.

Möller, A., O'Brien, P.J., Kennedy, A., Kröner, A., 2003. Linking growth episodes of zircon and metamorphic textures to zircon chemistry: an example from the ultrahigh-temperature granulites of Rogaland (SW Norway). In: Vance, D., Müller, W., Villa, I.M. (Eds), Geochronology: linking the isotopic record with petrology and textures. Geological Society, London, Special Publications 220, pp. 65-81.

Mulch, A., Cosca, M.A., Andresen, A., Fiebig, J., 2005. Time scales of deformation and exhumation in extensional detachment systems determined by high-spatial resolution in situ UV-laser $^{40}Ar/^{39}Ar$ dating. Earth and Planetary Science Letters 233, 375-390.

Olesen, O., Smethurst, M.A., Torsvik, T.H., Bidstrup, T., 2004. Sveconorwegian igneous complexes beneath the Norwegian-Danish Basin. Tectonophysics 387, 105-130.

Paludan, J., Hansen, U.B., Olesen, N.Ø., 1994. Structural evolution of the Precambrian Bjerkreim-Sokndal intrusion, South Norway. Norsk Geologisk Tidsskrift 74, 185-198.

Passchier, C.W., Myers, J.S., Kröner, A., 1990. Field geology of high-grade terrains. Springer-Verlag, Berlin, Heidelberg, 150 p.

Passchier, C.W., Trouw, R.A.J., 2005. Microtectonics (2^{d} Ed.). Springer-Verlag, Berlin, Heidelberg, xvi + 366 p.

Pasteels, P., Demaiffe, D., Michot, J., 1979. U-Pb and Rb-Sr geochronology of the eastern part of the south Rogaland igneous complex, southern Norway. Lithos 12, 199-208.

Pegrum, R.M., 1984. The extension of the Tornquist Zone in the Norwegian North Sea. Norsk Geologisk Tidsskrift 64, 39-68.

Pharaoh, T.C., 1999. Palaeozoic terranes and their lithospheric boundaries within the Trans-European Suture Zone (TESZ): a review. Tectonophysics 314, 17-41.

Rietmeijer, F.J.M., 1979. Pyroxenes from iron-rich igneous rocks in Rogaland, SW Norway. Geologica Ultraiectina 21.

Rochette, P., Jackson, M., Aubourg, C., 1992. Rock magnetism and the interpretation of anisotropy of magnetic susceptibility. Reviews of Geophysics 30, 209-226.

Román-Berdiel, T., Casas, A.M., Olivia-Urcia, B., Pueyo, E.L., Rillo, C., 2004. The main Variscan deformation event in the Pyrenees: new data from the structural study of the Bielsa granite. Journal of Structural Geology 26, 659-677.

Schärer, U., Wilmart, E., Duchesne, J.C., 1996. The short duration and anorogenic character of anorthosite magmatism: U-Pb dating of the Rogaland complex, Norway. Earth and Planetary Science Letters 139, 335-350.

Schlische, R.W., Withjack, M.O., 2009. Origin of fault domains and fault-domain boundaries (transfer zones and accomodation zones) in extensional provinces: result of random nucleation and self-organized fault growth. Journal of Structural Geology 31, 910-925.

Sigmond, E.M.O., 1985. The Mandal-Ustaoset line, a newly discovered major fault zone in south Norway. In: Tobi, A. C., Touret, J.L.R. (Eds), The deep Proterozoic crust in the North Atlantic Provinces. Reidel, Dordrecht, pp. 323-331.

Sigmond, E.M.O., Gustavson, M., Roberts, D., 1984. Berggrunnskart over Norge – 1:1000000. Norges geologiske undersøkelse.

Starmer, I.C., 1993. The Sveconorwegian orogeny in southern Norway, relative to deep crustal structures and events in the North Atlantic Proterozoic Supercontinent. Norsk Geologisk Tidsskrift 73, 109-132.

Streckeisen, A., 1974. How should charnockitic rocks be named? In: Bellière, J., Duchesne, J.C. (Eds.), Géologie des domaines cristallins. Société Géologique de Belgique, Liège, Volume du Centenaire, pp. 349-360.

Tobi, A.C., Hermans, G.A.E.M., Maijer, C., Jansen, J.B.H., 1985. Metamorphic zoning in the high-grade Proterozoic of Rogaland-Vest Agder, SW Norway. In: Tobi, A. C., Touret, J.L.R. (Eds.), The deep Proterozoic crust in the North Atlantic Provinces. Reidel, Dordrecht, pp. 477-497.

Tomkins, H.S., Williams, I.S., Ellis, D.J., 2005. *In situ* U-Pb dating of zircon formed from retrograde garnet breakdown during decompression in Rogaland, SW Norway. Journal of Metamorphic Geology 23, 201-215

Trindade, R.I.F., Raposo, M.I.B., Ernesto, M., Siqueira, R., 1999. Magnetic susceptibility and partial anhysteretic remanence anisotropies in the magnetite-bearing granite pluton of Tourão, NE Brazil. Tectonophysics 314, 443-468.

Vander Auwera, J., Bogaerts, M., Bolle, O., Longhi, J., 2008. Genesis of intermediate igneous rocks at the end of the Sveconorwegian (Grenvillian) orogeny (S Norway) and their contribution to intracrustal differentiation. Contributions to Mineralogy and Petrology 156, 721-743.

Vander Auwera, J., Bogaerts, M., Liégeois, J.P., Demaiffe, D., Wilmart, E., Bolle, O., Duchesne, J.C., 2003. Derivation of the 1.0-0.9 Ga ferro-potassic A-type granitoids of southern Norway by extreme differentiation from basic magmas. Precambrian Research 124, 107-148.

Vander Auwera, J., Bolle, O., Bingen, B., Liégeois, J.P., Bogaerts, M., Duchesne, J.C., De Waele, B., Longhi, J. Massif-type anorthosites and related granitoids result from post-collisional remelting of a continental arc root: the Sveconorwegian case. Submitted to Earth-Science Reviews.

Vander Auwera, J., Weis, D., Duchesne, J.C., 2006. Marginal mafic intrusions as indicators of downslope draining of dense residuals melts in anorthositic diapirs? Lithos 89, 329-352.

Westphal, M., Schumacher, J.C., Boschert, S., 2003. High-temperature metamorphism and the role of magmatic heat sources at the Rogaland anorthosite complex in Southwestern Norway. Journal of Petrology 44, 1145-1162.

Wilmart, E., Duchesne, J.C., 1987. Geothermobarometry of igneous and metamorphic rocks around the Åna-Sira anorthosite massif: implications for the depth of emplacement of the South Norwegian anorthosites. Norsk Geologisk Tidsskrift 67, 185-196.

Wilson, J.R., 1977. Farsundite – a suitable term for charnockite nomenclature? Neues Jahrbuch für Mineralogie, Monatshefte, H. 7, 324-331.

Wilson, J.R., Robins, B., Nielsen, F.M., Duchesne, J.C., Vander Auwera, J., 1996. The Bjerkreim-Sokndal layered intrusion, Southwest Norway. In: Cawthorn, R.G. (Ed.), Layered intrusions. Elsevier, Amsterdam, pp. 231-255.

Zhou, X.Q., Bingen, B., Demaiffe, D., Liégeois, J.P., Hertogen, J., Weis, D., Michot, J., 1995. The 1160 Ma Hidderskog meta-charnockite: implication of this A-type pluton for the Sveconorwegian belt in Vest-Agder (SW Norway). Lithos 36, 51-66.

Figure captions

Fig. 1. (a) Sketch map of the western portion of the Sveconorwegian orogen (simplified from Bingen *et al.*, 2005; offshore data after Andersson *et al.*, 1996; Pharaoh, 1999; Olesen *et al.*, 2004; inset map of Fennoscandia modified after Bogdanova *et al.*, 2008); RVA, Rogaland–Vest-Agder sector; MUL, Mandal-Ustaoset Line; Fl, Id and Bo are Flå, Iddefjorden and Bohus granites. (b) Geological map of the Rogaland–Vest-Agder sector (after Sigmond *et al.*, 1984; Mandal-Ustaoset Line and isograds from Falkum, 1982; Tobi *et al.*, 1985; Bingen *et al.*, 1996; boundaries for the Rogaland anorthosite province and the Farsund intrusion from references listed in the caption of Fig. 2). Pig-, Osm-, Opx- and Cpx-in are pigeonite-, osumilite-, orthopyroxene- and clinopyroxene-in isograds; Fe and Ma, Feda and Mandal gneisses; EGOG, Hå, He and ÅS are Egersund-Ogna, Håland, Helleren and Åna-Sira anorthosites; BKSK and Ap, Bjerkreim-Sokndal layered intrusion and its Apophysis; Hi and Ga, Hidra and Garsaknatt leuconorites; Ly1 and Ly2, main body and northern limb of the Lyngdal granodiorite; Ho, Holum monzogranite. Ages quoted in the legend were compiled from available U-(Th)-Pb geochronological data (see text for references).

Fig. 2. Geological and structural map of the Farsund intrusion and its surroundings. Modified after Falkum *et al.* (1979), Krause and Pedall (1980), Falkum (1982, 1998) and Marker *et al.* (2003). Most structural measurements in the Farsund pluton and close to its margins are from this study. A contoured equal-area projection (lower hemisphere; contours at 1-2-4-6-8-10 %) shows the distribution of the foliation poles in the Farsund intrusion. “Igneous” fabric, as opposed to gneissic fabric, refers to the fabric observed in the igneous bodies, irrespective of the degree of solid-stated deformation superimposed on the magmatic fabric. The concordant gneisses have steeply-dipping foliations and, based on locally available measurements,

gently- to moderately- or steeply-plunging mineral lineations that are parallel to the structures measured in neighbouring strongly-foliated rocks from the Farsund intrusion and the Rogaland anorthosite province. The axial plane traces of large-scale folds in the gneisses, as shown to the north of the Farsund intrusion, belong to the F2 to F5 folding phases of Falkum (1998). The limit of the area labelled "Quaternary moraines" corresponds to an approximate boundary of a coastal plain covering the bedrock.

Fig. 3. Distribution map of the lithofacies, constructed from combined microscope and field observations. AMS sampling sites are located. Other samples are from Dupont (2004), and Vander Auwera and Bolle (work in progress). An approximate boundary between AMC and HBG zones is drawn in the Farsund intrusion. This boundary is primary a limit between Opx and Hbl + Bt samples; some Hbl + Opx samples were integrated in the HBG zones, on the basis of chemical analyses conducted at or close to the sampling site.

Fig. 4. Photomicrographs (transmitted light, crossed nicols) illustrating microscope-scale evidence of ductile deformation in the Farsund intrusion and the Lyngdal granodiorite. (a) chessboard pattern in a quartz grain, defined by square-shaped subgrains (Opx + Hbl sub-facies, site 54; Table 1); (b) quartz grain with elongated subgrains, fringed with aggregates of small quartz grains probably developed by dynamic recrystallization, in a sample from the Lyngdal granodiorite collected at ca. 600 m from the contact with the Farsund intrusion (site 41; Table 1); (c) plagioclase grain with curved polysynthetic twins (Opx + Hbl sub-facies, site 89; Table 1); (d) slight kinking of a primary orthopyroxene grain (Opx + Hbl sub-facies, site 48; Table 1); (e) irregular quartz (above) vs. microperthitic orthoclase (below) grain boundary (Opx + Hbl sub-facies, site 49; Table 1); (f) quartz ribbons and dynamically recrystallized matrix in a sample from the Hidra mylonitic zone (Opx + Hbl sub-facies, site 27; Table 1).

Fig. 5. (a) Partial histograms of the bulk magnetic susceptibility (K_m); (b) Contoured map of K_m. See remark in Table 1.

Fig. 6. (a) Plot of Jelinek's (1981) AMS anisotropy degree (P_j) vs. bulk magnetic susceptibility (K_m) (strongly-strained rocks come from the Hidra mylonitic zone and from areas of strain localization in the Farsund shear zone); (b) Jelinek's (1981) plot of AMS shape (T_j) vs. anisotropy degree (P_j); (c) Contoured map of P_j; (d) Contoured map of T_j. See remark in Table 1.

Fig. 7. (a) Map of the magnetic foliations, with contoured equal-area projections of the foliation poles (lower hemispheres; contours at 1-2-4-6-8-10 % for the Farsund intrusion and 1-6-12 % for the Lyngdal granodiorite). Gneissic foliations and some "igneous" foliations from Fig. 2 are also shown. (b) Contoured map of the magnetic foliation dips, with foliation trajectories. Gneissic and "igneous" foliations from Fig. 2 were combined with the magnetic foliations to draw the trajectories. In the high-grade gneisses to the NE of the Farsund intrusion, only the trajectories of the concordant, steeply-dipping foliations, as found close to the pluton margin, are drawn (for more structural details in the area, see Fig. 2). Subvertical foliation has dip ≥ ca. 80°. See also the remark in Table 1.

Fig. 8. (a) Map of the magnetic lineations, with contoured equal-area projections (lower hemispheres; contours at 1-3-6-9-12 % for the Farsund intrusion and 1-8-16 % for the Lyngdal granodiorite). Most mineral lineations from Fig. 2 are also shown. (b) Contoured map of the magnetic lineation plunges, with lineation trajectories. Mineral lineations from

Fig. 2 were combined with the magnetic lineations to draw the trajectories. See also the remark in Table 1.

Fig. 9. (a) Schematic structural map of the Rogaland anorthosite province (RAP), Farsund intrusion and adjacent areas, highlighting foliation trajectories. Simplified from references quoted in the caption of Fig. 2, Rietmeijer (1979), Paludan *et al.* (1994), Jorde *et al.* (1995), Bolle *et al.* (2000) and Fig. 7b. Foliation trajectories are drawn from foliation and igneous layering in the anorthosite-leuconorite bodies, igneous modal layering in the cumulates of the Bjerkreim-Sokndal layered intrusion (BKSK), and “igneous” and magnetic foliations in the Farsund intrusion and the Lyngdal granodiorite (see Fig. 7), as well as in the BKSK felsic rocks and the Apophysis. In the BKSK, the planar fabric in the felsic rocks is concordant to a penetrative foliation (S_1) overprinting the original layering (S_0) in the cumulates; this S_1 foliation is usually parallel to S_0 in the limbs of the lobes formed by the folded cumulates and, hence, it is not drawn in these areas. The concordant steeply-dipping gneisses correspond to the belts of concordant gneisses defined on Fig. 2 and to their northern extension. (b) Comparison of the lineation pattern found in the present study (right) with that evidenced in the BKSK (left; drawn from magnetic lineations and, in the cumulates, mineral lineations, after Paludan *et al.*, 1994 and Bolle *et al.*, 2000). The Central Zone in the BKSK felsic rocks is an area where the lineation plunges are universally very steep (average orientation of N62E/87NE).

Figure 1

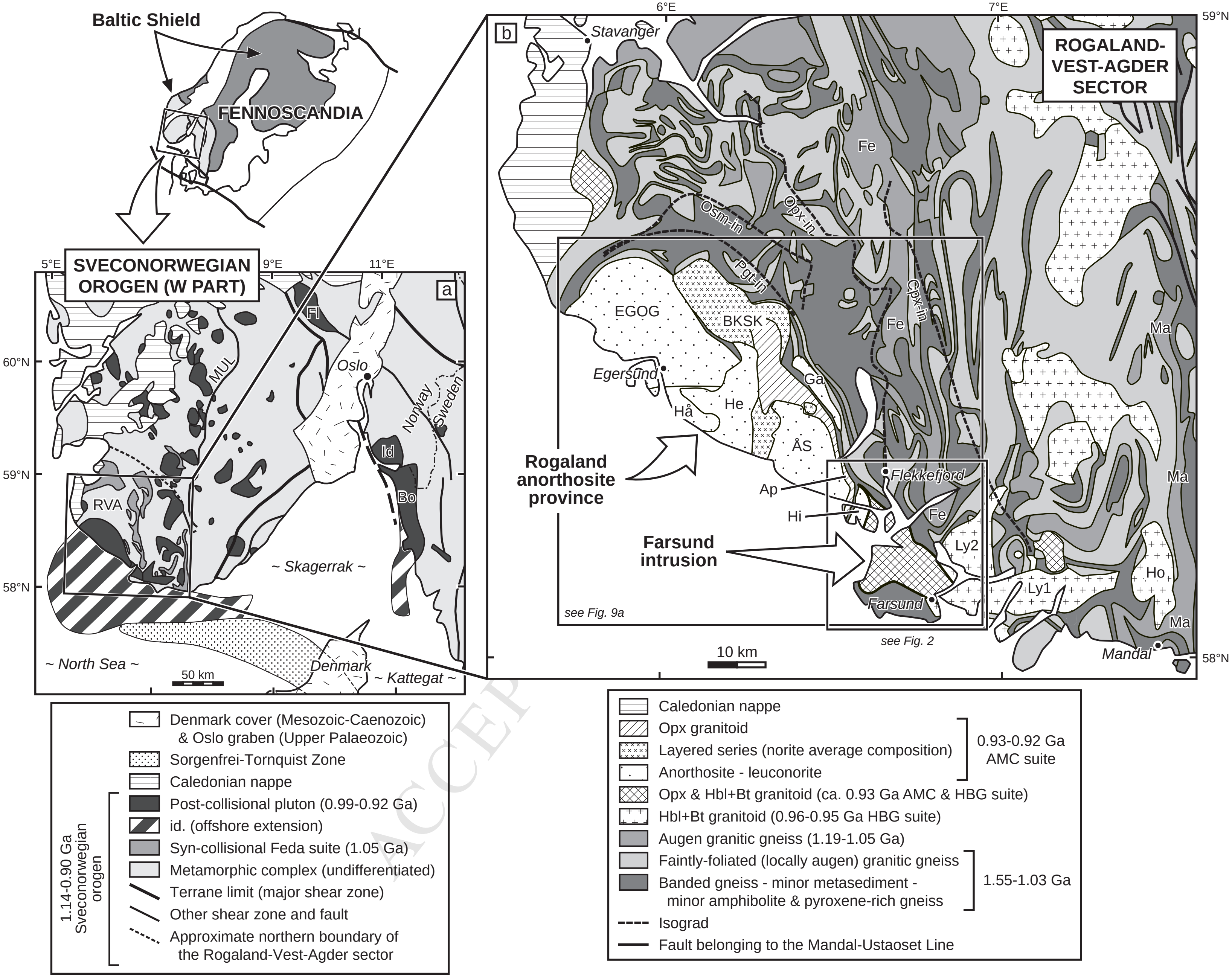

Fig. 1 - Bolle *et al.*

Figure 2

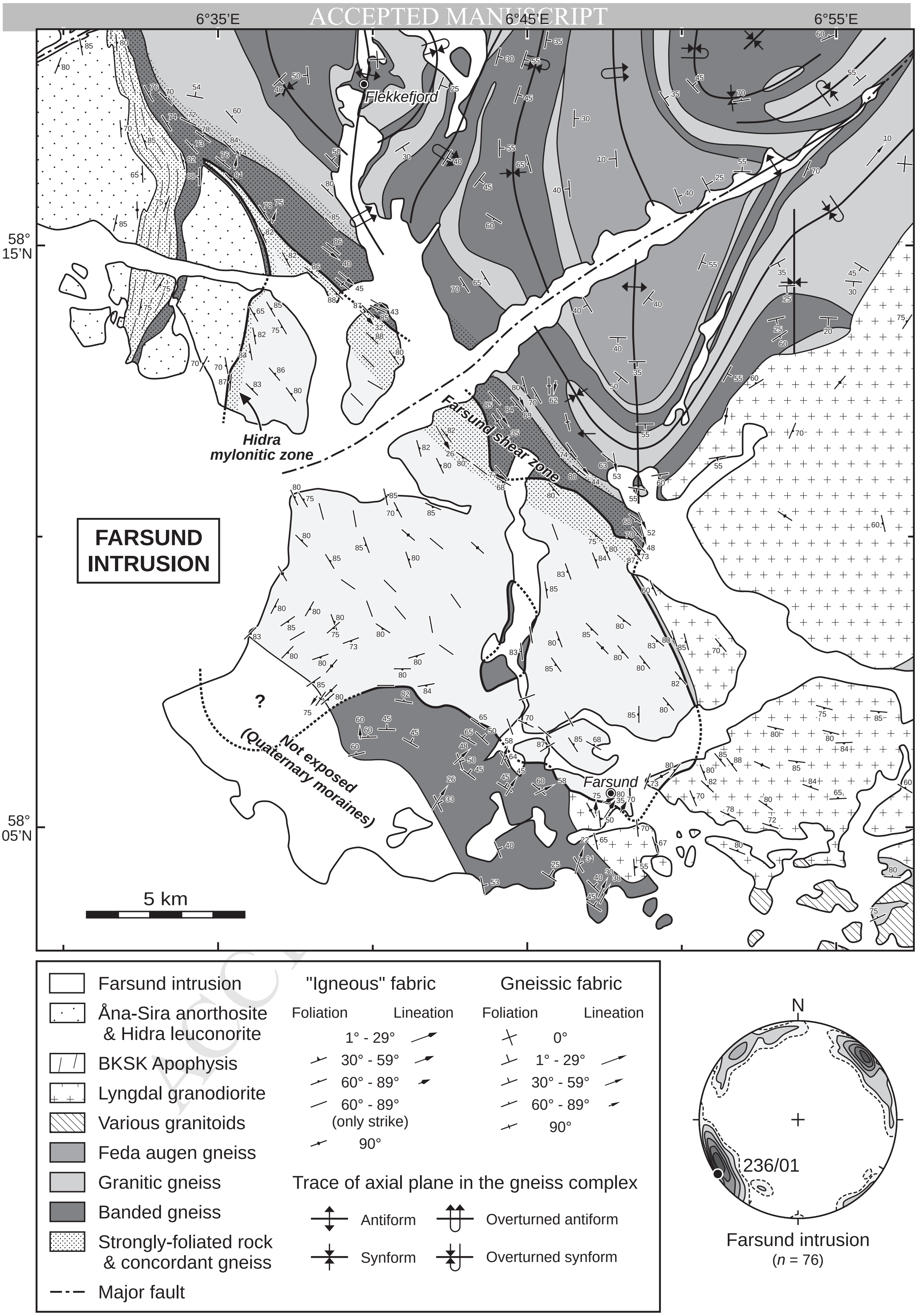

Fig. 2 - Bolle *et al.*

Figure 3

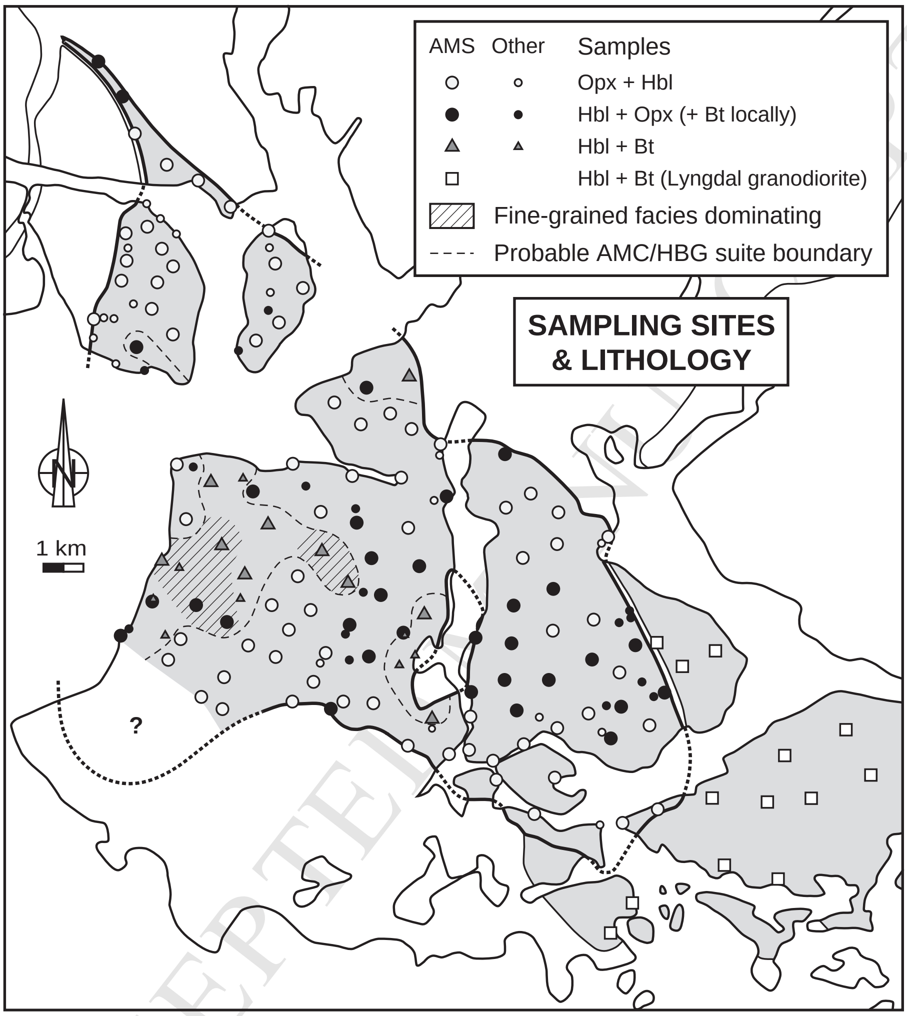

Fig. 3 - Bolle *et al.*

Figure 4

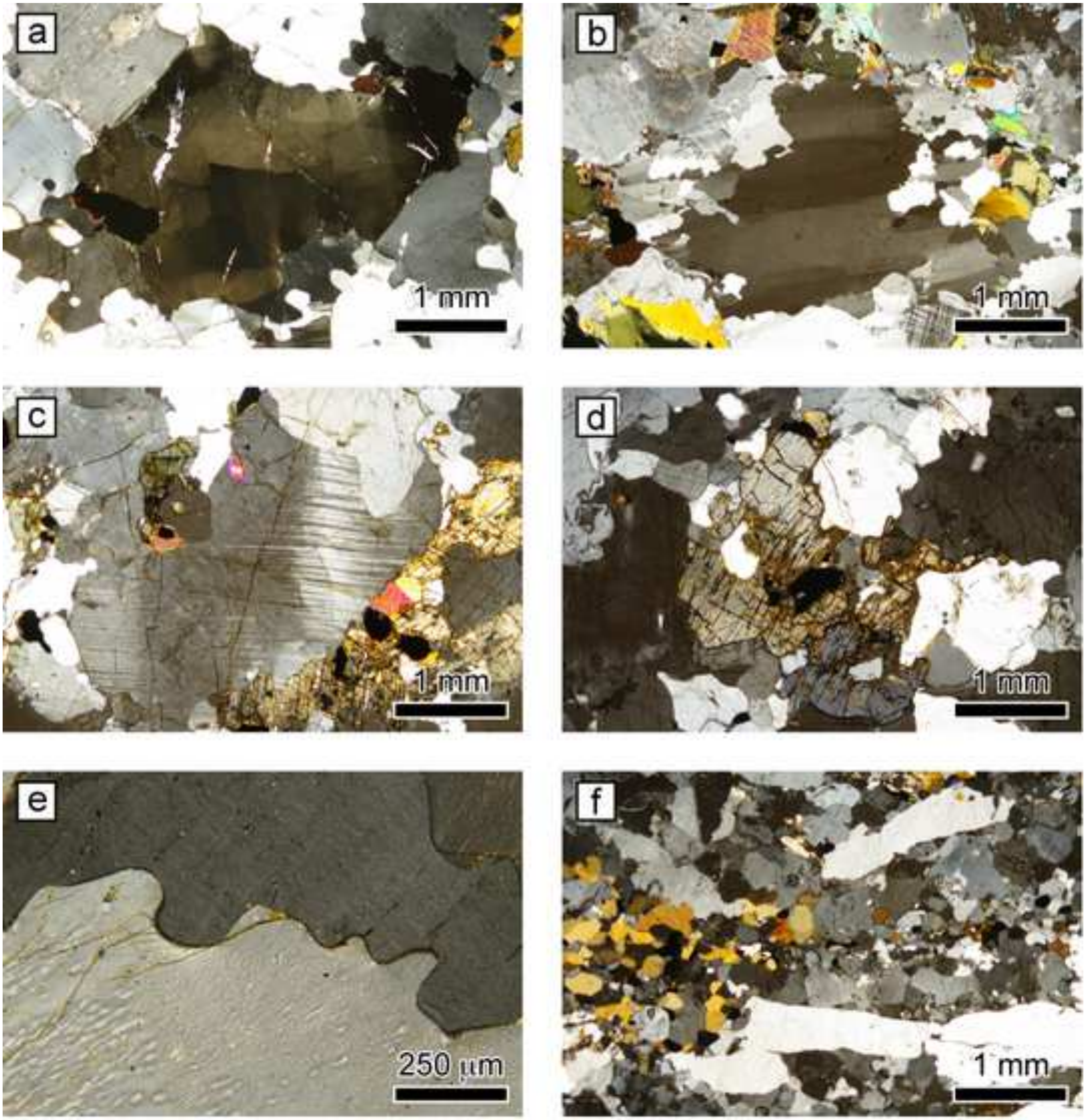

Fig. 4 - Bolle *et al.*

Figure 5

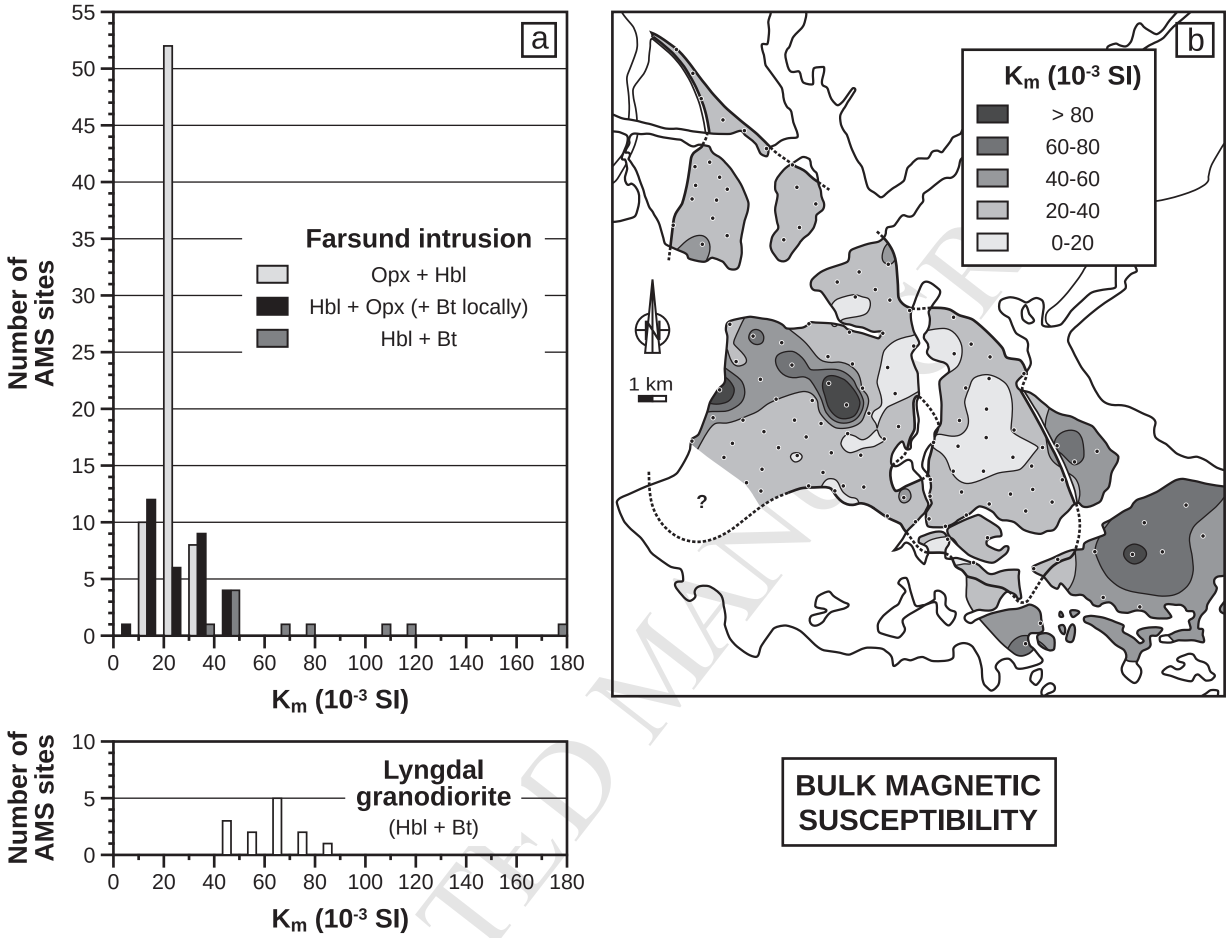

Fig. 5 - Bolle *et al.*

Figure 6

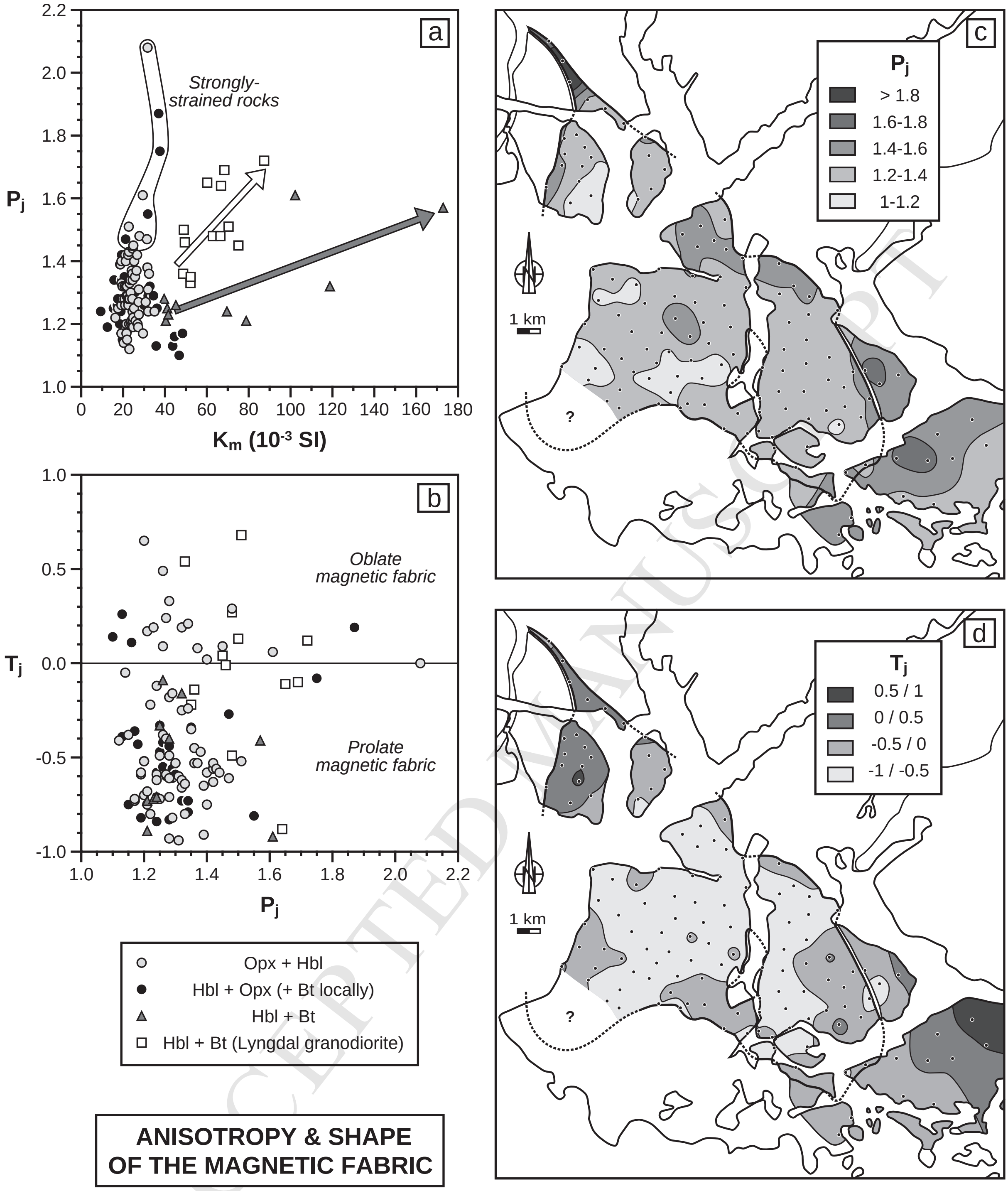

Fig. 6 - Bolle *et al.*

Figure 7

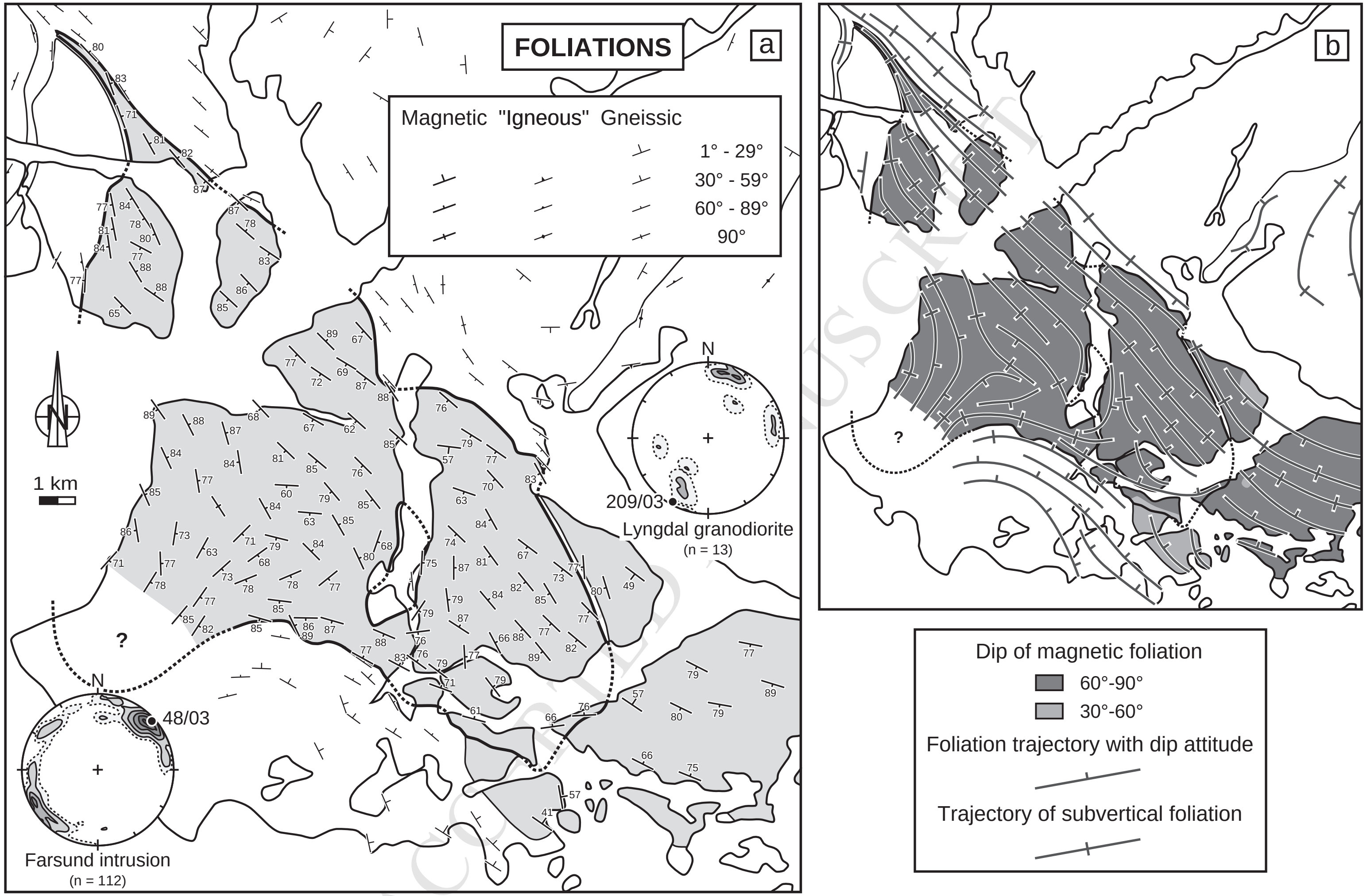

Fig. 7 - Bolle *et al.*

Figure 8

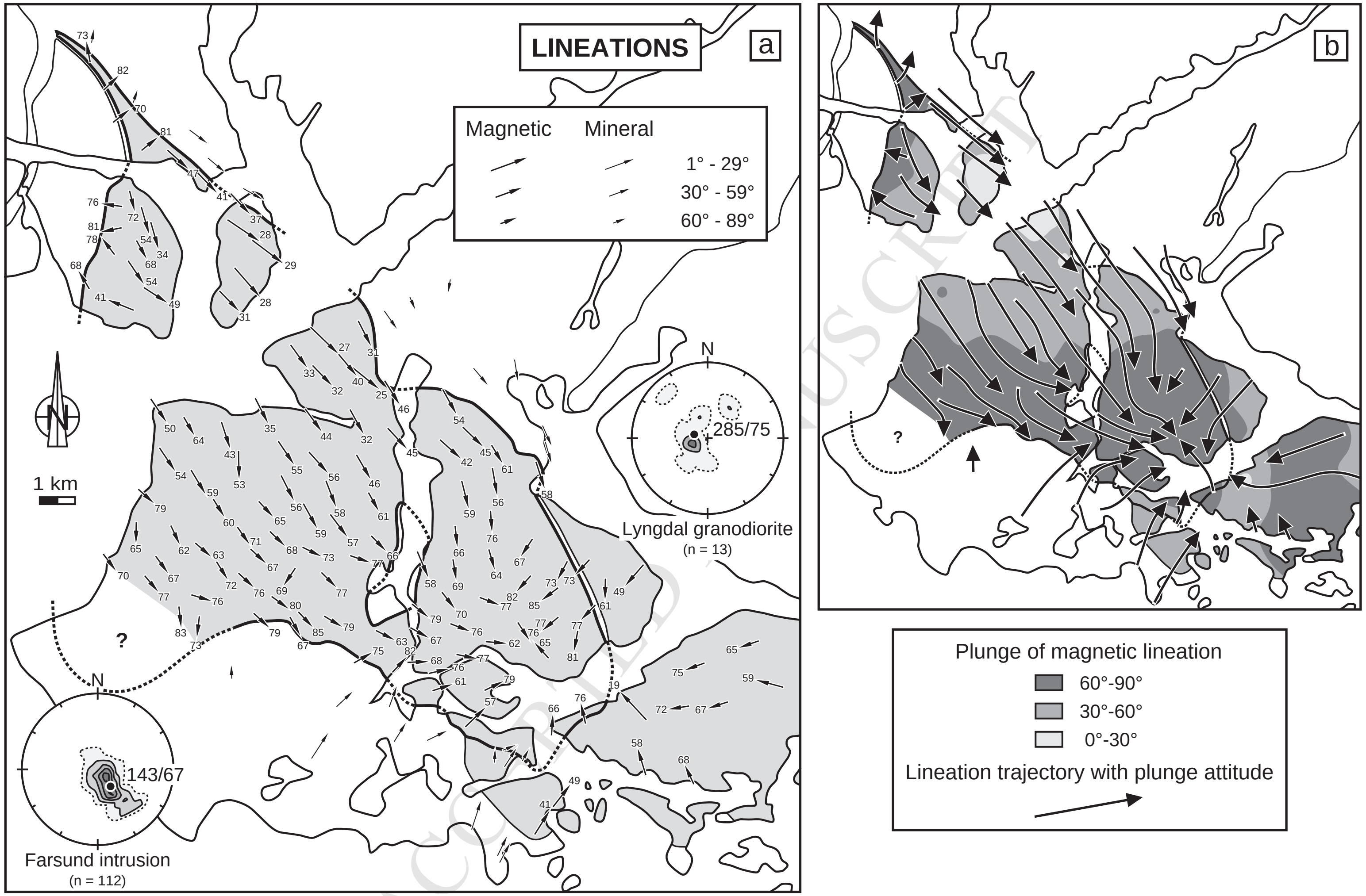

Fig. 8 - Bolle *et al.*

Figure 9

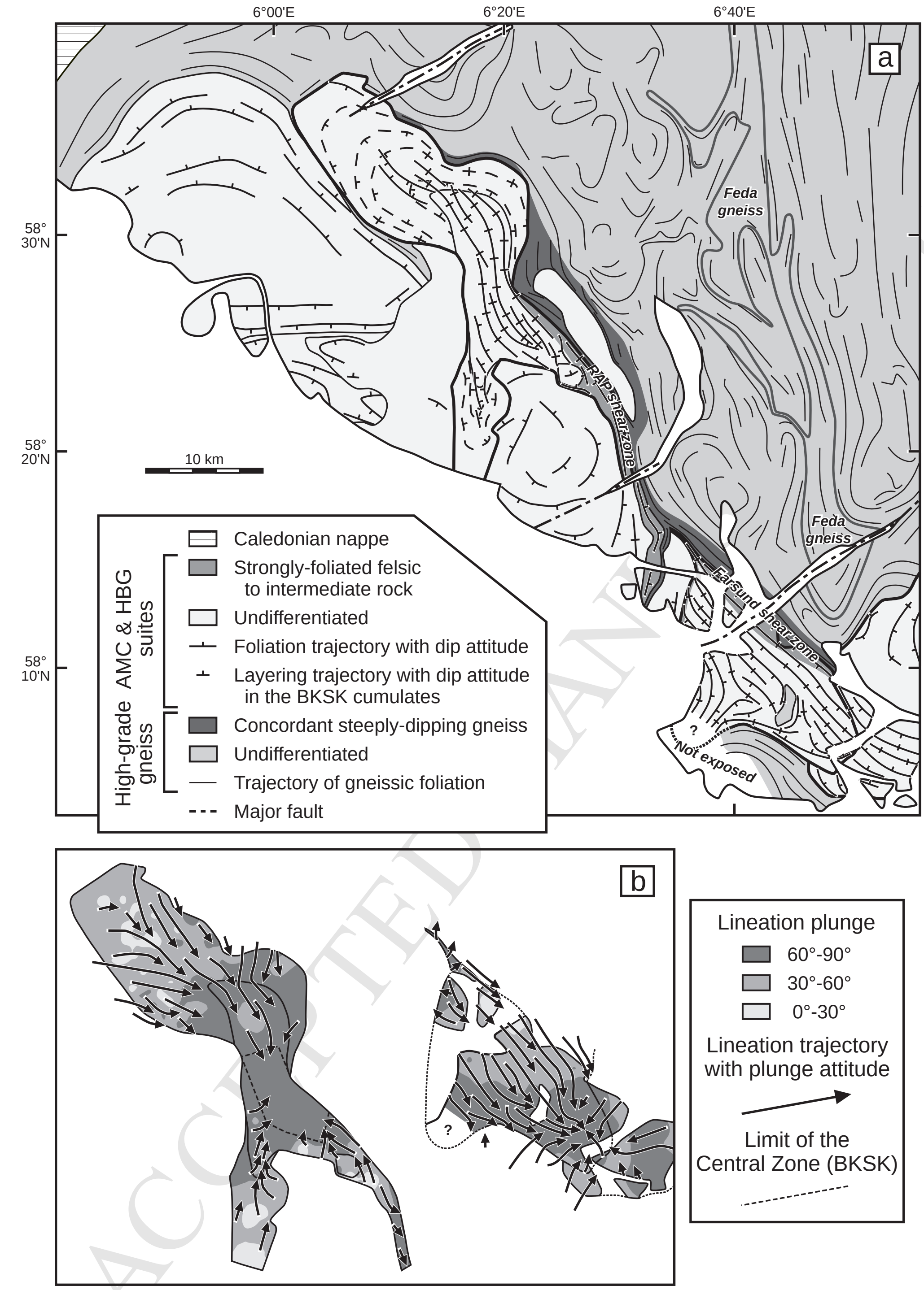

Fig. 9 - Bolle *et al.*

Table 1

Table 1. AMS data

Site	n	X	Y	Type	K_m	P_j	T_j	K_1 Dec	K_1 Inc	K_3 Dec	K_3 Inc
1	4	58325	54700	Opx + Hbl (c)	29.4	1.61	0.06	329	68	93	13
2	4	59046	55637	Opx + Hbl (c)	24.9	1.45	0.09	323	78	82	6
3	4	59186	56116	Opx + Hbl (c)	19.7	1.32	0.19	259	81	79	9
4	4	59173	56812	Opx + Hbl (c)	25.3	1.40	0.02	278	76	79	13
5	4	59745	56978	Opx + Hbl (c)	27.5	1.23	0.19	166	72	58	6
6	4	60085	56390	Opx + Hbl (c)	22.5	1.28	0.33	164	54	57	12
7	4	60358	55951	Opx + Hbl (c)	26.0	1.21	0.17	164	34	67	10
8	4	59951	55553	Opx + Hbl (c)	22.5	1.26	0.49	151	68	28	13
9	4	66941	51244	Opx + Hbl (c)	22.7	1.51	-0.52	148	46	56	2
10	4	67022	49925	Hbl + Opx (c)	19.5	1.34	-0.79	137	45	42	5
11	4	65835	50435	Opx + Hbl (c)	21.5	1.32	-0.66	151	32	42	28
12	4	64714	50539	Opx + Hbl (c)	22.4	1.42	-0.56	144	44	30	23
13	4	63232	50846	Opx + Hbl (c)	24.1	1.37	-0.53	153	35	47	22
14	4	62517	49402	Hbl (c)	78.8	1.21	-0.73	179	53	81	6
15	4	62130	50219	Hbl + Opx (c)	48.4	1.17	-0.36	162	43	254	3
16	4	61118	50453	Hbl (c)	69.6	1.24	-0.71	150	64	243	2
17	4	60270	50905	Opx + Hbl (c)	24.7	1.21	-0.68	146	50	55	1
18a	6	61352	48841	Hbl (f)	37.5	1.28	-0.87	154	60	264	11
b	2			Hbl (c)	51.9	1.15	-0.30	139	53	257	19
	8			(average)	41.6	1.23	-0.72	149	59	261	13
19	4	71048	48771	Opx + Hbl (c)	24.4	1.28	-0.71	162	58	61	7
20	4	69719	48625	Opx + Hbl (c)	18.7	1.39	-0.65	170	56	48	20
21	4	67670	46339	Hbl + Opx (c)	17.5	1.28	-0.83	157	58	273	15
22	4	68596	47100	Hbl + Opx (c)	25.6	1.30	-0.59	174	66	44	16
23	4	69600	47500	Hbl + Opx (c)	9.3	1.24	-0.72	176	76	61	6
24	4	61845	57428	Opx + Hbl (c)	23.5	1.34	0.21	136	41	43	3
25	4	61075	58082	Opx + Hbl (c)	30.8	1.27	0.24	132	47	230	8
26	4	59242	60301	Hbl + Opx (c)	37.0	1.87	0.19	46	82	250	7
27	4	59566	59362	Opx + Hbl (c)	31.7	2.08	0.00	52	70	250	19
28	4	60260	58548	Opx + Hbl (c)	26.4	1.37	0.08	51	81	241	9
29	4	58625	61224	Hbl + Opx (c)	37.6	1.75	-0.08	350	73	227	10
30	4	64482	46766	Hbl + Opx (c)	18.4	1.20	-0.70	116	73	225	6
31	4	63875	46025	Opx + Hbl (c)	24.8	1.19	-0.59	214	69	337	12
32	4	63563	45295	Opx + Hbl (c)	21.9	1.15	-0.38	126	80	7	5
33	4	62625	45964	Opx + Hbl (c)	19.2	1.17	-0.73	133	76	338	12
34	4	61911	46272	Opx + Hbl (c)	21.5	1.20	-0.70	148	72	318	17
35	4	61267	44678	Opx + Hbl (c)	22.8	1.28	-0.61	187	73	303	8
36	4	61345	45505	Opx + Hbl (c)	24.8	1.22	-0.80	107	76	305	13
37	4	60715	45019	Opx + Hbl (c)	35.0	1.24	-0.62	174	83	310	5
38	3	60248	46536	Opx + Hbl (c)	23.0	1.12	-0.41	144	67	268	13
39	4	59928	45980	Opx + Hbl (c)	26.9	1.20	-0.52	140	77	302	12
40a	6	58782	46644	Hbl + Opx (c)	55.8	1.10	0.47	151	68	318	21
b	4			Hbl + Opx (f)	33.2	1.25	0.05	149	69	309	20
c	4			Hbl + Opx (MME)	34.5	1.36	-0.16	133	74	301	16
	14			(average)	44.6	1.16	0.11	143	70	312	19
41	4	73461	42125	Hbl + Bt + Ttn (L)	60.2	1.65	-0.11	317	19	214	33
42	4	72065	41895	Opx + Hbl (c)	21.9	1.32	-0.25	347	76	177	14
43	4	71183	41556	Opx + Hbl (c)	31.4	1.47	-0.61	4	66	172	24
44	4	68956	41820	Opx + Hbl (c)	19.8	1.28	-0.18	46	57	195	29
45	4	67993	43157	Opx + Hbl (c)	25.7	1.35	-0.35	77	76	217	11
46	4	68737	43548	Opx + Hbl (c)	27.5	1.31	-0.94	101	77	267	13
47	4	69521	42711	Opx + Hbl (c)	31.9	1.31	-0.60	64	79	233	11
48	4	67363	43419	Opx + Hbl (c)	23.1	1.28	-0.49	88	68	216	14
49	4	67422	44302	Opx + Hbl (c)	24.5	1.24	-0.59	119	67	353	14
50	4	67470	44925	Hbl + Opx (c)	34.5	1.29	-0.56	129	79	304	11
51	4	66869	43373	Opx + Hbl (c)	23.1	1.33	-0.64	43	82	208	7
52	4	68062	42688	Opx + Hbl (c)	17.6	1.25	-0.72	72	61	200	19
53	4	69615	43963	Opx + Hbl (c)	27.2	1.19	-0.58	95	62	242	24
54	4	70385	44343	Opx + Hbl (c)	32.4	1.36	-0.53	147	76	48	2
55	4	71198	44488	Hbl + Opx (c)	22.3	1.28	-0.44	230	77	44	13
56	4	72299	44817	Hbl + Opx (c)	19.3	1.42	-0.55	224	77	46	13
57	4	62800	56800	Opx + Hbl (c)	27.8	1.48	0.29	137	37	44	3
58	4	62930	55945	Opx + Hbl (c)	23.6	1.30	-0.53	124	28	221	12
59	4	63609	55300	Opx + Hbl (c)	32.0	1.24	-0.12	127	29	34	7
60	4	62987	54441	Opx + Hbl (c)	22.4	1.27	-0.40	139	28	47	4
61	2	62397	54003	Opx + Hbl (c)	22.9	1.20	-0.52	136	31	43	5
62	4	59360	53972	Hbl + Opx (c)	46.8	1.10	0.14	292	41	46	25
63	4	60279	54250	Opx + Hbl (c)	20.3	1.14	-0.05	123	49	215	2
64	4	59757	54897	Opx + Hbl (c)	23.9	1.20	0.65	146	54	239	2
65	4	59571	47494	Hbl + Opx (c)	43.7	1.13	-0.39	181	65	81	4
66a	4	59836	48496	Hbl + Ttn (c)	60.9	1.07	0.68	208	63	70	21
b	4			Hbl + Bt + Ttn (f)	156.4	1.37	-0.17	129	79	246	5
	8			(average)	118.8	1.32	-0.16	132	79	246	5
67	4	60482	49559	Opx + Hbl (c)	29.5	1.17	-0.72	146	54	245	6
68	6	61934	48103	Hbl (c)	40.4	1.21	-0.89	148	60	57	0
69	6	61424	46887	Hbl + Opx (f)	30.0	1.26	-0.42	131	63	299	27
70	6	60677	47360	Hbl + Opx (f)	36.2	1.25	-0.47	155	62	279	17
71	4	65055	44692	Opx + Hbl (c)	19.2	1.26	-0.38	121	79	16	3
72	4	64282	44767	Opx + Hbl (c)	24.6	1.34	-0.24	137	85	1	4
73	2	66510	44281	Hbl + Bt (f)	45.2	1.26	-0.09	117	63	23	2
74	4	65830	43653	Opx + Hbl (c)	24.4	1.36	-0.45	60	75	209	13
75	4	64786	49343	Hbl + Opx (c)	32.0	1.29	-0.61	138	56	40	5
76	4	66040	49173	Opx + Hbl (c)	19.2	1.33	-0.80	150	46	45	14
77	4	66286	48158	Hbl + Opx (c)	15.7	1.34	-0.73	151	61	52	5
78	4	66391	46949	Hbl + Bt (c)	39.6	1.28	-0.40	136	66	289	22
79	4	65826	46435	Hbl + Opx (c)	19.7	1.15	-0.75	109	77	245	10
80	4	65095	48395	Hbl + Opx (c)	32.8	1.32	-0.73	159	58	50	11
81	4	64486	47824	Hbl + Bt + Ttn (f)	172.9	1.57	-0.41	151	59	5	27
82	4	65316	47466	Hbl + Opx (c)	18.9	1.24	-0.58	143	57	240	5
83	4	62959	46650	Opx + Hbl (c)	23.9	1.21	-0.75	133	67	324	22
84	4	63524	47151	Opx + Hbl (c)	21.6	1.17	-0.73	134	68	14	11
85	4	62569	47315	Opx + Hbl (c)	27.4	1.27	-0.59	145	71	315	19
86	4	63235	48007	Opx + Hbl (c)	20.7	1.28	-0.93	137	65	241	6
87	4	63879	48628	Bt + Ttn + Hbl (f)	102.2	1.61	-0.92	153	56	3	30
88	4	63845	49645	Opx + Hbl (c)	20.7	1.32	-0.62	146	55	44	9
89	4	62999	44783	Opx + Hbl (c)	25.2	1.25	-0.49	133	79	16	5
90	4	64963	45888	Hbl + Opx (c)	22.3	1.18	-0.43	135	77	321	13
91	4	66224	51642	Opx + Hbl (c)	24.6	1.44	-0.58	129	25	37	3
92	4	65684	52024	Opx + Hbl (f)	21.0	1.42	-0.63	140	40	31	21
93	4	64933	51781	Opx + Hbl (c)	19.2	1.40	-0.75	136	32	34	18
94	4	64297	52414	Opx + Hbl (c)	22.8	1.43	-0.56	144	33	46	13
95	4	65108	52728	Hbl + Bt + Opx (c)	31.8	1.55	-0.81	134	27	225	1
96	4	66151	52924	Hbl + Bt (c)	41.1	1.25	-0.33	153	31	48	23
97	4	68842	48297	Opx + Hbl (c)	21.6	1.29	-0.82	166	59	19	27
98	4	69789	49389	Opx + Hbl (c)	26.7	1.42	-0.53	149	61	35	13
99	4	69121	49935	Opx + Hbl (c)	21.3	1.40	-0.58	134	45	32	11
100	3	68482	49600	Opx + Hbl (c)	18.6	1.39	-0.91	132	42	7	33
101	4	68526	50920	Hbl + Opx (c)	21.2	1.47	-0.27	151	54	41	14
102	4	68611	44435	Hbl + Opx (c)	21.6	1.27	-0.60	111	76	213	3
103	4	68352	45242	Hbl + Opx + Bt (c)	18.5	1.24	-0.84	142	70	263	11
104	4	68527	46161	Hbl + Opx (c)	17.8	1.24	-0.71	171	69	270	3
105	6	69559	46454	Opx + Hbl (c)	16.3	1.22	-0.22	164	64	54	9
106	4	69433	45217	Hbl + Opx + Bt (c)	17.3	1.26	-0.55	111	77	230	6
107	4	70929	43633	Hbl + Opx (c)	35.8	1.13	0.26	318	65	51	1
108	4	63952	44650	Hbl + Opx (c)	12.5	1.19	-0.82	151	67	244	1
109	4	71346	39476	Hbl + Bt (L)	49.5	1.46	-0.01	38	49	260	33
110	4	70798	38751	Hbl + Bt (L)	66.5	1.48	-0.49	32	41	215	49
111	4	71204	45321	Opx + Hbl (c)	22.1	1.29	-0.16	233	85	59	5
112	4	70513	45667	Hbl + Opx (c)	15.4	1.25	-0.33	222	82	51	8
113	4	70605	46674	Opx + Hbl (c)	21.0	1.26	0.09	214	67	37	23
114	4	71618	46042	Hbl + Opx (c)	20.6	1.35	-0.34	208	73	38	17
115	4	71892	43949	Opx + Hbl (c)	31.6	1.38	-0.47	191	81	40	8
116	4	72773	45452	Hbl + Bt (L)	66.8	1.64	-0.88	181	61	73	10
117	4	72162	46078	Hbl + Bt (L)	68.4	1.69	-0.10	223	73	86	13
118	4	73661	45828	Hbl + Bt + Ttn (L)	49.0	1.50	0.13	221	49	37	41
119	4	74838	41948	Hbl + Bt + Ttn (L)	87.4	1.72	0.12	261	72	26	10
120	4	75296	43079	Hbl + Bt + Ttn (L)	62.9	1.48	0.27	250	75	27	11
121	4	76868	43681	Hbl + Bt + Ttn (L)	70.4	1.51	0.68	251	65	11	13
122	4	77476	42533	Hbl + Bt + Ttn (L)	52.2	1.33	0.54	285	59	17	1
123	4	75934	42029	Hbl + Bt + Ttn (L)	75.1	1.45	0.04	252	67	10	11
124	4	73680	40376	Hbl + Bt + Ttn (L)	48.7	1.36	-0.14	343	58	207	24
125	4	75085	39992	Hbl + Bt + Ttn (L)	52.3	1.35	-0.22	335	68	202	15

n: number of specimens; *X* and *Y*: coordinates (in m), in the WGS84 UTM grid (32V zone – LK (03E/64N) 100 km square); K_m: magnitude of the bulk magnetic susceptibility (in 10^{-3} SI); P_j and T_j: Jelinek's (1981) anisotropy degree and shape parameter; K_1 and K_3: long and short principal axes of the AMS ellipsoid (magnetic lineation and pole to the magnetic foliation, respectively); Dec and Inc: declination and inclination of the axes; Opx: orthopyroxene; Hbl: hornblende; Bt: biotite; Ttn: titanite; (c): coarse-grained facies; (f): fine-grained facies; (MME): mafic microgranular enclave; (L): Lyngdal granodiorite. Intermingled facies with contrasted grain sizes have been sampled at AMS sites 18, 40 and 66. For each of these three sites, the average values of the AMS parameters (K_m, P_j, T_j, K_1 Dec and Inc, K_3 Dec and Inc), as measured in the various facies, are considered in Figs 4-7. Such an averaging does not give any anomaly in the maps of Figs 4a, 5c-d, 6 and 7.